Fluctuating hydrodynamics of chiral active fluids

Ming Han,[1,2] Michel Fruchart,[1,3] Colin Scheibner,[1,3] Suriyanarayanan Vaikuntanathan,[1,4] Juan J. de Pablo,[2,5] and Vincenzo Vitelli[1,3,6,*]

[1] *James Franck Institute, University of Chicago, Chicago, Illinois 60637, U.S.A.*
[2] *Pritzker School of Molecular Engineering, University of Chicago, Chicago, Illinois 60637, U.S.A.*
[3] *Department of Physics, University of Chicago, Chicago, IL 60637, U.S.A.*
[4] *Department of Chemistry, University of Chicago, Chicago, IL 60637, U.S.A.*
[5] *Center for Molecular Engineering, Argonne National Laboratory, Lemont, Illinois 60439, U.S.A.*
[6] *Kadanoff Center for Theoretical Physics, University of Chicago, Chicago, IL 60637, U.S.A.*

Active materials are characterized by continuous injection of energy at the microscopic level and typically cannot be adequately described by equilibrium thermodynamics. Here, we study a class of active fluids in which equilibrium-like properties emerge when fluctuating and activated degrees of freedom are statistically decoupled, such that their mutual information is negligible. We analyse three paradigmatic systems: chiral active fluids composed of spinning frictional particles that are free to translate, oscillating granular gases, and active Brownian rollers. In all of these systems, a single effective temperature generated by activity parameterizes both the equation of state and the emergent Boltzmann statistics. The same effective temperature, renormalized by velocity correlations, relates viscosities to steady-state stress fluctuations via a Green-Kubo relation. To rationalize these observations, we develop a theory for the fluctuating hydrodynamics of these non-equilibrium fluids and we validate it through large-scale molecular dynamics simulations. Our work sheds light on the microscopic origin of odd viscosities and stress fluctuations characteristic of parity-violating fluids, in which mirror symmetry and detailed balance are broken.

Granular media have long been a playground for children and statistical physicists alike [1–3]. Here, we consider a class of non-equilibrium fluids exemplified by frictional grains constantly spinning in a plane. Typically, two grains of sand would only lose energy by friction when they collide. By contrast, spinning particles can also gain energy after a collision, if their rotation speed is rapidly reset to a constant value by microscopic torques or external fields. A collection of many such particles, all spinning in the same direction (clockwise or anticlockwise), is often referred to as a chiral active fluid [4–13]. Experimental realizations include colloidal particles [4, 11, 14], robots [10] and even living systems [15, 16]. In this article, we use non-equilibrium statistical mechanics to develop a fluctuating hydrodynamic theory for chiral active fluids: a continuum theory that describes both the macroscopic behaviour of the fluid and its fluctuations in one go. This allows us to describe phenomena ranging from steady-state velocity fluctuations to non-linear shock propagation.

Despite being driven and dissipative, chiral active fluids share several aspects with equilibrium fluids when their spinning speed is nearly constant and uniform. They display a Maxwell-Boltzmann probability distribution, an equation of state, and their viscous response satisfies a fluctuation-response relation. The same viscous response bears signatures of their non-equilibrium character through the existence of so-called odd viscosities that can only occur when detailed balance is broken. These equilibrium-like behaviours occur when the activated and fluctuating degrees of freedoms are statistically decoupled, a feature that we shall see extends beyond chiral active fluids to other systems such as oscillating granular gases [17–19] and active Brownian rollers [20, 21].

* Corresponding author: vitelli@uchicago.edu

Microscopic model of a chiral active fluid

We start by considering a simplified microscopic model of a two-dimensional chiral active fluid (Fig. 1a and Supplementary Movs. S1-S3) composed of athermal frictional particles all spinning in the same direction [4–8, 10–12]. In order to impart a fixed chirality to the system, we incorporate active torques into a standard model of granular disks (see Methods Sec. A and Ref. [22]). The positions $\mathbf{x}_i$ of the particles and their angular velocities $\mathbf{\Omega}_i$ then follow the equations of motion

$$m\ddot{\mathbf{x}}_i = \sum_{j\in N(i)} \mathbf{f}_{ij} \tag{1}$$

$$I\dot{\mathbf{\Omega}}_i = \boldsymbol{\tau}_i + \sum_{j\in N(i)} \mathbf{r}_{ij}\times\mathbf{f}_{ij} \tag{2}$$

in which m is the mass of the particles and I their moment of inertia. Each particle i interacts with its neighbors $j \in N(i)$ closer than its diameter d through a force

$$\mathbf{f}_{ij} = \underbrace{-k\,(d-r_{ij})\,\hat{\mathbf{r}}_{ij}}_{\mathbf{f}_{ij}^{\mathrm{c}}} + \underbrace{\gamma\,(-\mathbf{v}_{ij}+\mathbf{\Omega}_{ij}\times\mathbf{r}_{ij})}_{\mathbf{f}_{ij}^{\mathrm{nc}}} \tag{3}$$

in which the central force $\mathbf{f}_{ij}^{\mathrm{c}}$ models a soft repulsion between the disks, and the noncentral force $\mathbf{f}_{ij}^{\mathrm{nc}}$ models interparticle friction (Fig. 1a). The particles i and j are separated by a vector $\boldsymbol{r}_{ij} = \boldsymbol{x}_i - \boldsymbol{x}_j = r_{ij}\,\hat{\mathbf{r}}_{ij}$, the difference between their velocities $\mathbf{v}_k = \dot{\mathbf{x}}_k$ is $\mathbf{v}_{ij} = \mathbf{v}_i - \mathbf{v}_j$, and the average rotation speed of a pair of particles is

$\boldsymbol{\Omega}_{ij} = \hat{\mathbf{z}}\,(\Omega_i + \Omega_j)/2$. In addition, each particle experiences an active torque $\boldsymbol{\tau}_i = \gamma_{\rm rot}(\Omega - \Omega_i)\hat{\mathbf{z}}$ that tends to maintain a constant angular velocity $\Omega_i \approx \Omega$. When $\gamma_{\rm rot}$ is large, Ω_i relaxes to Ω faster than other time scales in the system, allowing the rotational degrees of freedom (that we call *activated*) to act as an effective bath for the translational ones (that we call *fluctuating*). Hence, one can replace $\boldsymbol{\Omega}_{ij} \to \Omega\,\hat{\mathbf{z}}$ in Eq. (1) while eliminating Eq. (2). Crucially, the non-central force $\mathbf{f}_{ij}^{\rm nc}$ violates parity: Eq. (1) is not invariant under the mirror reflection $x, y \to -x, y$ when $\Omega \neq 0$ (the system is chiral).

Effective temperature

We conduct molecular dynamics simulations of the chiral active fluid described by Eq. (1) in this limit. Despite being athermal and driven, the active fluid exhibits a single effective temperature $T_{\rm eff}$ that controls three properties typically associated with thermal equilibrium: (i) a Maxwell distribution of particle velocities (Fig. 1b) (ii) a nearly Boltzmann distribution of particle concentration in the presence of an external potential (Supplementary Figs. S1-S3) (iii) an ideal gas equation of state (Fig. 1c). Similar properties emerge in oscillating granular gases (in which z translations are activated while (x, y) translations are fluctuating, see Methods Sec. A, Extended Fig. E1 and Supplementary Movs. S4-S5) and fluids of active Brownian rollers (in which translations are activated and rotations are fluctuating, see Extended Fig. E2 and Supplementary Movs. S6-S7). In both cases an effective thermodynamic description emerges when the corresponding activated and fluctuating degrees of freedom are statistically decoupled.

The emergence of an effective temperature in the chiral active fluid can be captured by a mean-field approximation. As the interparticle vector $\hat{\mathbf{r}}_{ij}$ is random, the term $\boldsymbol{\Omega}_{ij} \times \hat{\mathbf{r}}_{ij}$ in Eq. (1) can be replaced by a white noise whose temperature is determined self-consistently (see Supplemantary Sec. II). As a result, the fluid follows a Langevin dynamics similar to a thermal fluid

$$m\ddot{\mathbf{x}}_i = \sum_{j \in N(i)} \mathbf{f}_{ij}^{\rm c} - \gamma_{\rm eff}\mathbf{v}_i + \tilde{\boldsymbol{\xi}}(t) \tag{4}$$

in which $T_{\rm eff}$ can be seen as the temperature of the effective bath. We show in Supplementary Sec. II that $\gamma_{\rm eff} = n\pi d^2\gamma$ and $\langle\tilde{\xi}_a(t)\tilde{\xi}_b(t')\rangle = 2\gamma_{\rm eff}k_{\rm B}T_{\rm eff}\delta_{ab}\delta(t-t')$ (see also Fig. S4). In the chiral active fluid, the thermal exchange with a bath is replaced with an exchange of kinetic energy between rotational and translational degrees of freedom during collisions (see Fig. 1a). Once a collision is over, the rotational speed Ω_i of each spinning particle is rapidly restored to Ω by the active torques $\boldsymbol{\tau}_i$. This process leads to a net gain or loss of energy until the translational degrees of freedom reach the effective temperature $T_{\rm eff}(\Omega)$ at which gain and loss are balanced on average. We show in the Supplementary Sec. II that in this case, $T_{\rm eff} \propto |\Omega|^{\alpha}$, where α is a non-universal exponent depending on $\mathbf{f}_{ij}^{c}$ with $4/3 \leq \alpha \leq 2$. Consistent with this prediction, simulations with a contact potential reveal a power-law behavior $T_{\rm eff} \propto |\Omega|^{1.54\pm0.02}$ over two decades. We emphasize that the mean-field approximation in Eq. (4) only captures single-particle properties controlled by $T_{\rm eff}$, but not the breaking of detailed balance. Hence, Eq. (1) is still needed to fully account for the transport properties, such as viscosities, that are affected by the parity-violating nature of collisions illustrated in Fig. 2.

Chiral hydrodynamics

The evolution of the velocity field $\mathbf{u}$ of the chiral active fluid is described by the Navier-Stokes equation

$$\rho \mathrm{D}_t\mathbf{u} = \boldsymbol{\nabla}\cdot\boldsymbol{\sigma} + \mathbf{f}_{\rm vol} \tag{5}$$

in which $\mathrm{D}_t = \partial_t + u_a\partial_a$ is the material derivative, $\boldsymbol{\sigma}$ is the stress tensor, $\mathbf{f}_{\rm vol}$ are external body forces, and $\rho = nm$ is the mass density (n is the number density). The stress tensor $\boldsymbol{\sigma}$ in Eq. (5) is composed of a steady-state part $\boldsymbol{\sigma}^{\rm ss}$ present even in the absence of any velocity gradient, and a viscous part $\sigma_{ab}^{\rm vis} = \eta_{abcd}\,\partial_d u_c$, where η_{abcd} is the viscosity tensor of the fluid. The viscous stress $\sigma_{ab}^{\rm vis}$ describes surface forces between fluid layers that arise in response to velocity gradients. It is convenient to express the stress σ_{ab} and the unsymmetrized strain rate $\dot{e}_{cd} = \partial_d u_c$ as two vectors σ_α and $\dot{e}_\beta$ respectively, so that η_{abcd} can be represented as a matrix $\eta_{\alpha\beta}$ (see Methods Sec. B and Refs. [23, 24]). For an isotropic two-dimensional fluid, the constitutive relation between stress and strain rate reads

$$\begin{pmatrix} \sigma_{xx}+\sigma_{yy} \\ \sigma_{xy}-\sigma_{yx} \\ \sigma_{xx}-\sigma_{yy} \\ \sigma_{xy}+\sigma_{yx} \end{pmatrix} = \begin{pmatrix} -P \\ -\tau \\ 0 \\ 0 \end{pmatrix} + \begin{pmatrix} \zeta & \eta^{\rm B} & 0 & 0 \\ \eta^{\rm A} & \eta^{\rm R} & 0 & 0 \\ 0 & 0 & \eta & \eta^{\rm o} \\ 0 & 0 & -\eta^{\rm o} & \eta \end{pmatrix} \begin{pmatrix} \dot{e}_{xx}+\dot{e}_{yy} \\ \dot{e}_{xy}-\dot{e}_{yx} \\ \dot{e}_{xx}-\dot{e}_{yy} \\ \dot{e}_{xy}+\dot{e}_{yx} \end{pmatrix} \tag{6}$$

$$\sigma_\alpha \qquad \sigma_\alpha^{\rm ss} \qquad \eta_{\alpha\beta} \qquad \dot{e}_\beta$$

The velocity gradients $\dot{e}_\beta$ are decomposed into dilation, rotation, and two pure shears at 45° of each other, while the stress σ_α is decomposed into pressure, torque, and two shear stresses (see Methods Sec. B for explicit expressions).

We performed large-scale molecular dynamics simulations to determine both the equations of state of the chiral active fluid in the steady-state, and its viscous response to velocity gradients (Fig. 1e). In the simulations, the stress tensor $\boldsymbol{\sigma}$ is determined using the Irving–Kirkwood formula [27]

$$\sigma_{ab} = -\frac{1}{A}\left[\sum_i m v_i^a v_i^b + \frac{1}{2}\sum_{i\neq j} f_{ij}^a r_{ij}^b\right] \tag{7}$$

that expresses the stress tensor $\boldsymbol{\sigma}$ in terms of the trajectories of the individual particles and their microscopic interactions. Here, A is the total area of the system, i, j label particles, and a, b label spatial directions. The first

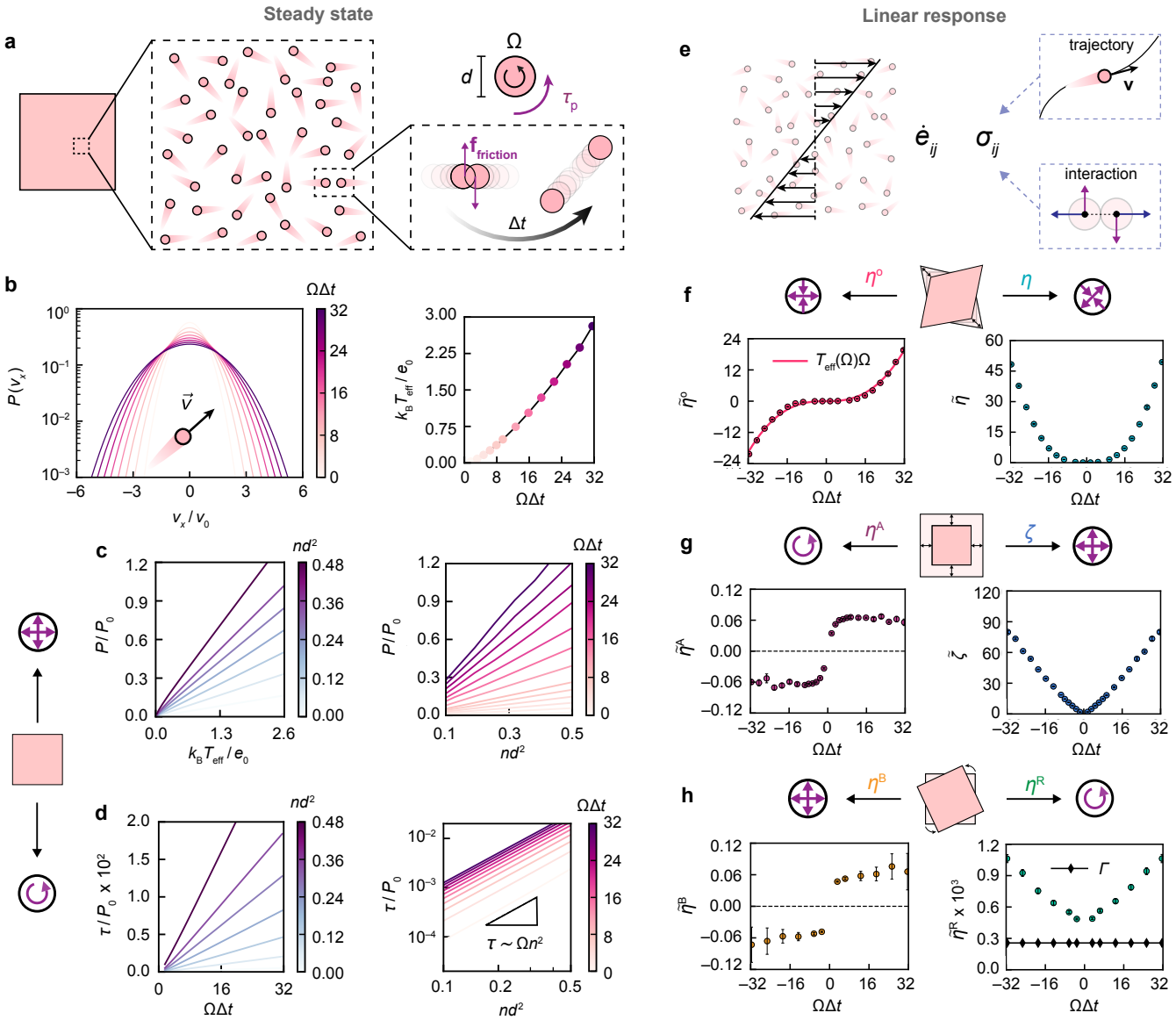

FIG. 1. **Steady state and linear response of a chiral active fluid. a.** Schematic of a granular gas. We simulate a 2D granular gas composed of frictional particles with diameter d, which are powered by an active torque τ_p to self-spin at a constant speed Ω. During collision, two self-spinning particles slide with respect to each other. The resultant interparticle friction causes transverse motion of the particles upon separation (Supplementary Mov. S1). $\Delta t = \sqrt{m/k}$ is a proxy for the average collision duration. **b.** Velocity distribution. The x-component of translational velocity follows a Gaussian distribution $P(v_x)$ at various spinning speeds Ω. An effective temperature $T_{\rm eff}$ is defined using the variance of v_x. The dependence of $T_{\rm eff}$ on Ω is shown on the right. **c-d.** Equations of state. At the steady state, this system acquires an effective pressure P that satisfies the ideal gas law, $P = nk_{\rm B}T_{\rm eff}$, where n is particle density. Unlike thermal systems, it also acquires a nonvanishing torque density τ that satisfies the relation $\tau \sim \Omega n^2$. **e.** Schematic of rheological measurements. We perturb the system with a velocity gradient $\dot{e}_{k\ell} = \partial_\ell u_k$ and measure the stress σ_{ij} to infer the viscosity tensor $\eta_{ijk\ell}$. The stress is calculated in the bulk from particle trajectory and interactions using the Irving–Kirkwood formula Eq. (7). This method can be applied to either simulation or experimental data. In the dilute limit, the kinetic part of the Irving–Kirkwood formula dominates, so the stress tensor can be determined purely from movies of particle motion, without knowledge of microscopic interactions. **f.** Odd and shear viscosities. A pure shear induces shear stress s_1 (⊕) via odd viscosity $\eta^{\rm o}$ and shear stress s_2 (⊗) via shear viscosity η. **g.** Compression-rotation and bulk viscosities. A dilation/compression alters the torque density τ (↻) via a compression-rotation viscosity $\eta^{\rm A}$ and the pressure P (⊕) via the bulk viscosity ζ. **h.** Rotation-Compression and rotation-rotation viscosities. A rotation changes the pressure P (⊕) via a rotation-compression viscosity $\eta^{\rm B}$ and the torque density τ (↻) via a rotation-rotation viscosity $\eta^{\rm R}$. The coefficient $\Gamma = \tau/\Omega$ is plotted as a comparison. The dependencies of all the viscosities on spinning speed Ω are shown in **f-h**. The diagonal terms η, ζ, and $\eta^{\rm R}$ in Eq. (6) are even in Ω, while $\eta^{\rm A}$, $\eta^{\rm B}$, and $\eta^{\rm o}$ are odd in Ω. Besides, $\eta^{\rm A}(\Omega) = -\eta^{\rm B}(-\Omega)$. All the viscosities $\tilde{\eta}_a = \eta_a/\eta_0$ are in units of $\eta_0 = m/d\Delta t$. We have defined $v_0 = d/\Delta t$, $e_0 = md^2/\Delta t^2$, and $P_0 = m/[d\Delta t^2]$. Unless otherwise specified, the number density is $nd^2 = 0.254$. Error bars denote standard errors.

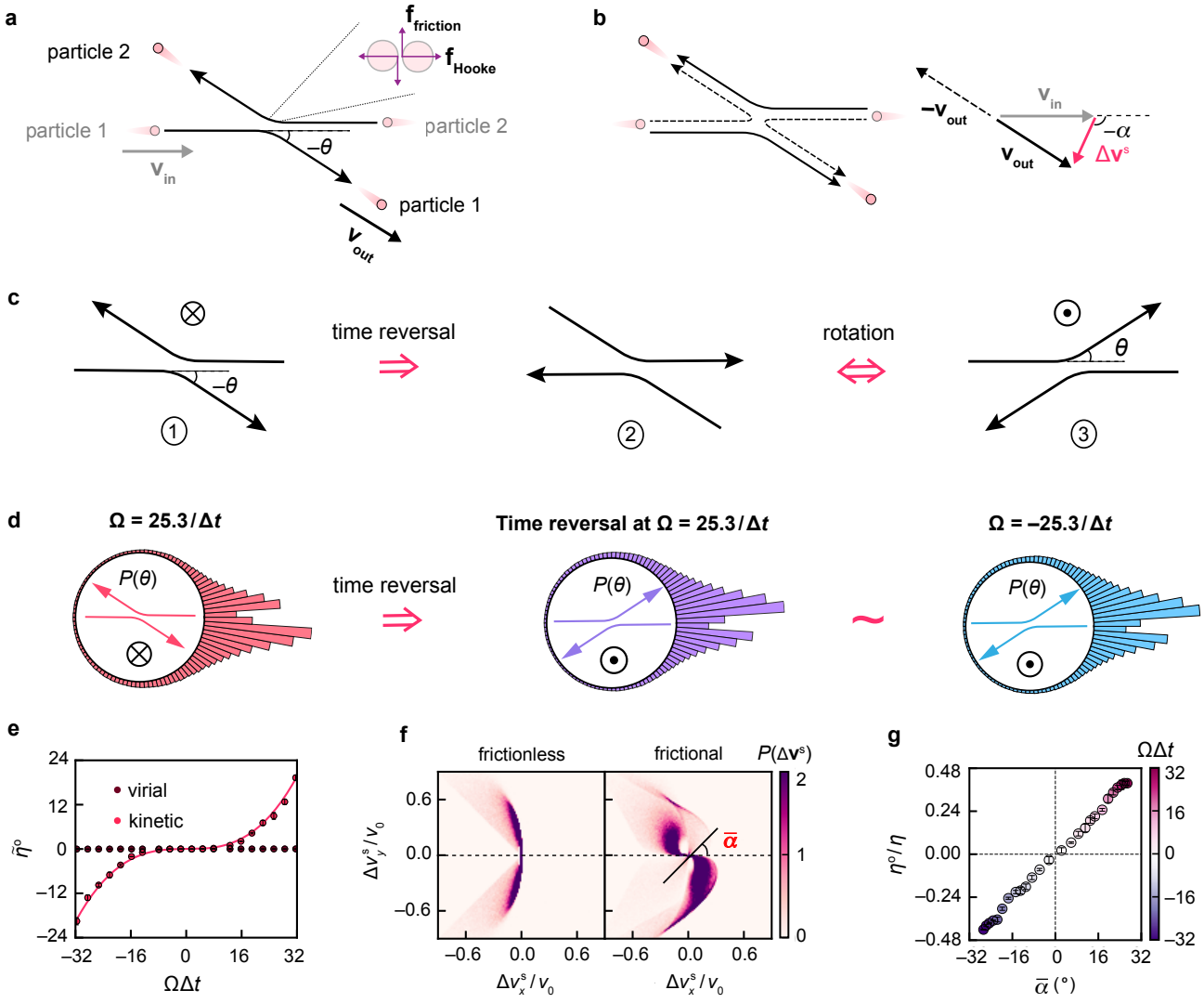

FIG. 2. **Parity-violating collisions and microscopic origin of odd viscosity.** Transport coefficients of our dilute granular gas such as its viscosity are mainly determined by the two-particle collision kernel. **a.** Consider a collision between two particles 1 and 2. In the center of mass reference frame, they have incoming velocities $\pm\mathbf{v}_{\text{in}}$ and outgoing velocities $\pm\mathbf{v}_{\text{out}}$. The scattering angle is defined as $\theta = \text{angle}(\mathbf{v}_{\text{in}}, \mathbf{v}_{\text{out}})$. **b.** As the particles are identical, we can always assume that $\pm\mathbf{v}_{\text{in}} \cdot \pm\mathbf{v}_{\text{out}} \geq 0$. We then introduce the velocity change $\Delta\mathbf{v} = \mathbf{v}_{\text{out}} - \mathbf{v}_{\text{in}}$ and the angle $\alpha = \text{angle}(\mathbf{v}_{\text{in}}, \Delta\mathbf{v})$, which are directly related to the momentum exchanged between the particles during the collision. **c.** The non-central interaction between two active spinners with surface friction breaks the symmetry between θ and $-\theta$ (see also Supplementary Mov. S1), or equivalently between α and $-\alpha$. For positive (negative) self-spinning speeds, the particle coming from left turns slightly downward (upward). In other words, the collisions are chiral. This can be seen by comparing a given collision (①) with the time-reversed collision ($\mathbf{v} \to -\mathbf{v}$, see ②). We can use isotropy to fix the direction of $\mathbf{v}_{\text{in}}$. The rotated time-reversed collision ③ differs from the original one ①. **d.** This is quantitatively measured by the scattering angle distributions $P(\theta)$. The scattering angle distribution at self-spinning speed Ω_0 is therefore different from the distribution at $-\Omega_0$. However, it is identical to the time-reversed of the angle distributions at $-\Omega_0$. This suggests that at the steady-state, the time-reversed dynamics is statistically equivalent to the dynamics with reversed self-spinning speed. **e.** Contribution of the virial and kinetic stresses to odd viscosity η^{o} (see Eq. (7)). The kinetic part dominates in our dilute granular gas. The number density is $nd^2 = 0.254$. **f.** Distribution of the symmetrized velocity change $P(\mathbf{\Delta v}^{\text{s}})$. When the particles are frictionless ($\boldsymbol{f}_{ij}^{\text{nc}}$ set to zero), collisions do not break parity. When the particles are frictional, the collisions are chiral and $P(\mathbf{\Delta v}^{\text{s}})$ displays a chiral distortion with a characteristic twisting angle $\bar{\alpha}$ defined as the average of the angle α in panel **b**. This twisting angle gives a measure of the parity-violating nature of the collisions. **g.** The odd viscosity ratio η^{o}/η is proportional to the twisting angle $\bar{\alpha}$. (A similar direct quantitative relation doesn't exist for the average scattering angle.) Error bars denote standard errors.

term in Eq. (7) is called the kinetic part, and the second is called the virial part. We find that in addition to a standard isotropic pressure P following the ideal gas law $P = nk_{\rm B}T_{\rm eff}$ (Fig. 1c), the steady-state stress tensor $\boldsymbol{\sigma}^{\rm ss}$ exhibits an anti-symmetric part (odd stress) corresponding to the net torque density $\tau = \Gamma(n)\Omega$ with a density dependent rotational friction coefficient $\Gamma(n) \sim n^2$ (Fig. 1d, extended Fig. E3). This antisymmetric stress would not arise from purely radial pairwise interactions between the particles, even if they were subject to microscopic torques [28]. Instead, it is a hydrodynamic manifestation of the transverse part of the force $\mathbf{f}_{ij}$ in Eq. (3). To see that, let us compute from Eq. (7) the antisymmetric part of the Irving-Kirkwood stress [corresponding to the second line in Eq. (6)]

$$\sigma_{ab} - \sigma_{ba} = \epsilon_{ab} \left[\frac{1}{2A} \sum_{i \neq j} \mathbf{r}_{ij} \times \mathbf{f}_{ij} \right] \tag{8}$$

in which only the virial part contributes as $v_i^a v_i^b = v_i^b v_i^a$. This shows that pairwise interactions can only contribute to the antisymmetric part of the stress when they are not central (i.e., when $\mathbf{r}_{ij} \times \mathbf{f}_{ij} \neq 0$). The force $\mathbf{f}_{ij}$ in Eq. (3) is short-ranged, so it affects the system only during collisions. Since the collision rate scales with the square of the density n, the cumulative effect of the gear-like frictional forces results in the observed $\Gamma(n) \sim n^2$.

Linear response: even and odd viscosities

All the entries of the viscosity matrix were determined by deforming the simulation box at constant strain rate using the SLLOD algorithm [29]. The results (Fig. 1f-h and Supplementary Figs. S5-S7) are consistent with the general form Eq. (6) imposed by isotropy. In addition to the standard shear and bulk viscosities η and ζ, we observe additional viscosity coefficients allowed by the broken time-reversal and parity. First, a coefficient $\eta^{\rm o}$ known as odd (or Hall) viscosity [9, 11, 24, 30–37] couples the two shear stresses. The ratio $\eta^{\rm o}/\eta$, of order one, is directly related to the angle $\overline{\alpha}$ defined in Fig. 2. This angle characterizes the average chirality of the collisions, which arises from the parity-violating interaction $\mathbf{f}_{ij}^{\rm nc}$ in Eq. (1). In addition, we find other parity-violating viscosities $\eta^{\rm A}$ and $\eta^{\rm B}$ that couple compression and rotation, and have smaller but nonzero magnitudes. Besides, there is a viscous contribution $\eta^{\rm R}\omega$ to the antisymmetric stress, where $\omega = \dot{\phi}$ is the vorticity. In an equilibrium fluid, we would have $\eta^{\rm R} = -\Gamma$ [28, 38], but this is not the case here (Fig. 1h). As they lead to an antisymmetric stress, the coefficients $\eta^{\rm A}$, $\eta^{\rm R}$ and Γ can only come from the virial contribution to Irving-Kirkwood stress [see Eq. (8)]. In a dilute gas, this contribution is usually small compared to the kinetic part since collisions are rare. In contrast, the shear viscosities are typically dominated by the kinetic part of the stress in dilute gases, and essentially independent of the density, consistent with our findings (see Fig. 1f-h and Fig. 2e, Supplementary Fig. S8).

Comparing the linear response of chiral active fluids with opposite Ω, we find that up to numerical uncertainty $\eta^{\rm o}$, $\eta^{\rm A}$ and $\eta^{\rm B}$ are odd function of Ω while η, ζ and $\eta^{\rm R}$ are even functions (Fig. 1f-h). Moreover, $\eta^{\rm A}(\Omega) \approx -\eta^{\rm B}(-\Omega)$ (Fig. 1g-h). These relations imply (but are not equivalent to) $\eta_{abcd}(\Omega) = \eta_{dcba}(-\Omega)$. These results are reminiscent of Onsager–Casimir reciprocity relations that would occur in an equilibrium fluid [39, 40]. The existence of these relations can be understood from the statistical properties of interparticle collision and symmetry considerations (see Supplementary Sec. VI). First, the breaking of parity is parameterized by Ω. The system at $-\Omega$ is equivalent to the one at Ω under a mirror reflection $P_x = \mathrm{diag}(-1, 1)$, which changes the sign of the parity-violating viscosities including $\eta^{\rm A}$, $\eta^{\rm B}$ and $\eta^{\rm o}$ but does not affect the remaining viscosities. Second, although each individual collision is not time-reversal invariant, the time-reversed collisions at Ω are on average equivalent to the collisions at $-\Omega$ (Fig. 2d). This indicates that near the steady state, there is a correspondence between the time-reversed dynamics at Ω and the time-forward dynamics at $-\Omega$ in the statistical sense. From this, we can show that the relations $\eta_{abcd}(\Omega) = \eta_{dcba}(-\Omega)$ hold, see Supplementary Sec. VI.

We also find that odd viscosity follows the relation $\eta^{\rm o} \sim T_{\rm eff}(\Omega)\,\Omega$ (Fig. 1f) while the shear viscosity $\eta(T_{\rm eff})$ depends on Ω only through the effective temperature (Supplementary Fig. S6). In extended Fig. E4, we present the results of large-scale molecular dynamics simulations of a non-linear compression shock: the transverse macroscopic flow induced by odd stress and odd viscosity is directly visible (Supplementary Mov. S8). Quantitative comparison between numerics and theory corroborates our hydrodynamic description of this chiral active fluid (see also Supplementary Figs. S9-S11).

Fluctuating hydrodynamics

We now turn to the fluctuating hydrodynamics of the chiral active fluid. Standard fluid mechanics is deterministic. However, fluctuations of the hydrodynamic variables must be taken into account in situations such as the onset of phase transitions and hydrodynamic instabilities, and in turbulent flows. They also determine the correlation functions of the fluid, that in turn control physical properties such as light scattering [41, 42]. To describe these fluctuations, let us go back to the Navier-Stokes Eq. (5) and add to the stress tensor $\boldsymbol{\sigma}$ a fluctuating component $\boldsymbol{\sigma}^{\rm R}$ with zero mean in addition to the steady-state and viscous components in Eq. (6). In our chiral active fluid, we find that the correlations of the random stress are of the form

$$\left\langle \sigma_\alpha^{\rm R}(\mathbf{r}, t)\, \sigma_\beta^{\rm R}(0, 0) \right\rangle = 2k_{\rm B}T_{\rm eff}\, \delta(\mathbf{r}) \Big[\eta_{\alpha\beta}^{\rm sym}\delta(t) + \eta_{\alpha\beta}^{\rm anti}\xi(t) \Big] \tag{9}$$

in which $\eta_{\alpha\beta}^{\rm sym(anti)}$ is the symmetric (antisymmetric) part of the matrix η under index exchange $\alpha \leftrightarrow \beta$, $\delta(t) = \delta(-t)$ is a symmetric function of time peaked at $t = 0$ and $\xi(t) = -\xi(-t)$ is an antisymmetric function peaked

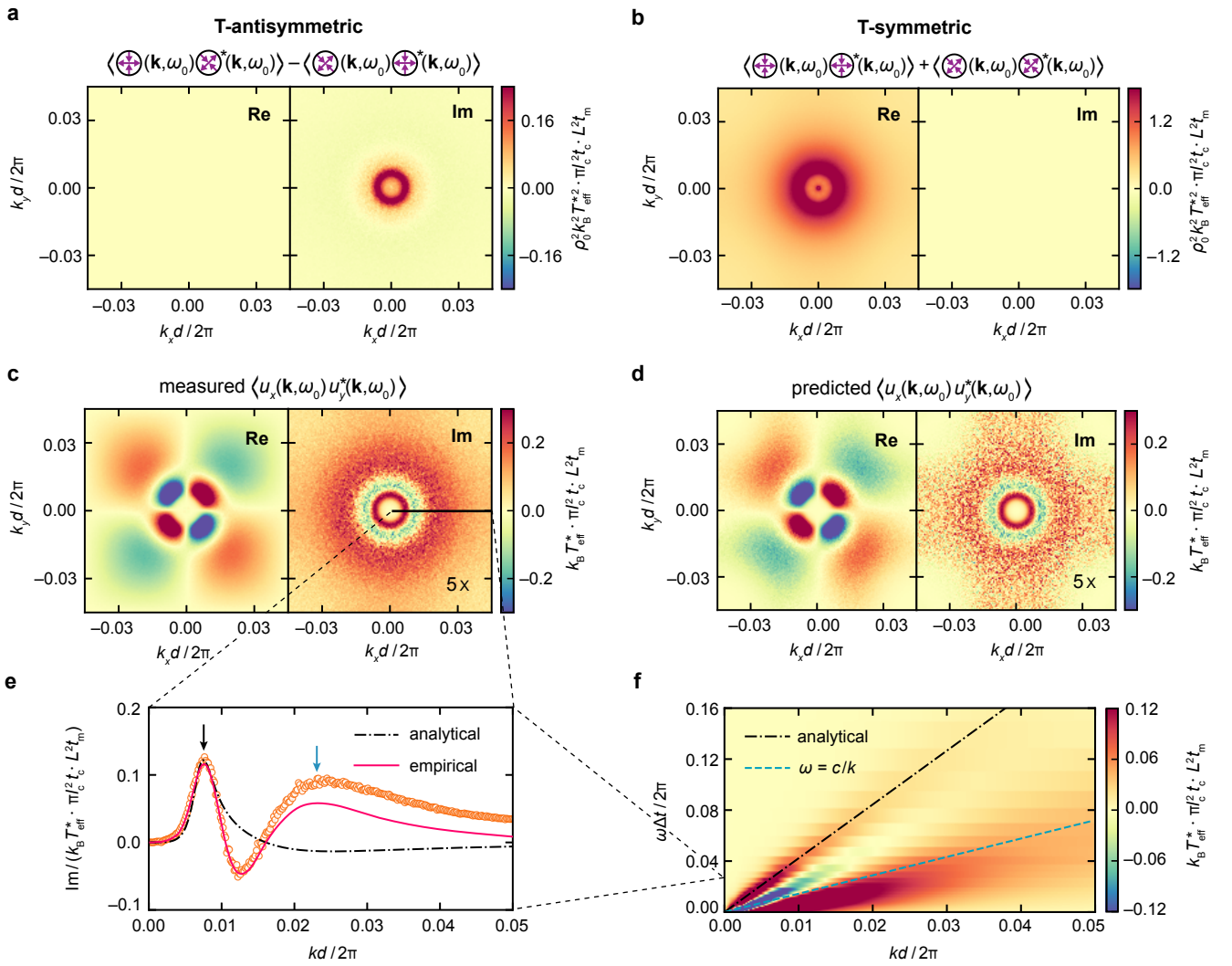

FIG. 3. **Fluctuating hydrodynamics of chiral active fluids.** The stress-stress correlations **a,b** and velocity-velocity correlations **c** were obtained from direct measurements in molecular dynamics simulations, and compared in **d** and **e** with the predictions of the fluctuating hydrodynamic theory. Panels **a-e** correspond to a fixed excitation (wave) frequency $\omega = \omega_0 \equiv 0.055\pi/\Delta t$ (but different wavevectors $\mathbf{k}$). In **f**, we plot the excitation spectrum of the system as a function of the frequency ω and the wave mode $k = |\mathbf{k}|$. **a-b.** Stress–stress correlation functions. The purely imaginary combination $2\,\mathrm{i}\,\mathrm{Im}\langle s_1 s_2^*\rangle$ plotted in **a** is antisymmetric under time-reversal (TR), and is associated with odd viscosity η^{o}. The purely real component $\langle s_1 s_1^*\rangle + \langle s_2 s_2^*\rangle$ plotted in **b** is TR-symmetric, and is associated with shear viscosity η. **c-d.** Velocity–velocity correlation functions. We compare the correlation function $c_{xy}(\mathbf{k},\omega) = \langle u_x(\mathbf{k},\omega) u_y^*(\mathbf{k},\omega)\rangle$ measured in particle-based simulation (**c**) with the one predicted using our fluctuating hydrodynamic theory (**d**) using the stress-stress correlations measured in **a-b**. The real part corresponds to the effects of η, whereas the imaginary part corresponds to η^{o}. In **c** and **d**, the imaginary parts are magnified 5 times for readability. **e.** Radially averaged velocity correlation function $\mathrm{Im}\big[c_{xy}(k,\omega)\big]$. We compare the simulation data (orange points) with (i) an analytical solution (black dashed line) obtained from the linearized fluctuating hydrodynamic theory in which all time scales in the stress correlations are neglected by replacing $\delta(t)$ in Eq. (9) with a Dirac distribution (and similarly for ξ) and (ii) an empirical solution (red solid line) obtained from the measured momentum-dependent viscosity and stress–stress correlation functions (Supplementary Figs. S16-S17). The simplified analytical solution (i) assumes a constant viscosity tensor and applies only in the hydrodynamic limit: it indeed captures the first peak at $k_1 = 0.015\pi/d$ of the velocity correlation function in **e**. The empirical estimation (ii) also captures the second peak at $k_2 = 0.047\pi/d$, which was completely missed by the linear theory. The first and second peaks are marked with black and blue arrows, respectively. **f.** Power spectrum of $\mathrm{Im}\big[c_{xy}(k,\omega)\big]$. Our theoretical prediction on the position of the first peak (black dashed line) applies to a wide range of frequencies ω. We also find that the second peak is associated with the dispersion relation of the fluid $\omega = ck$ (cyan dashed line).

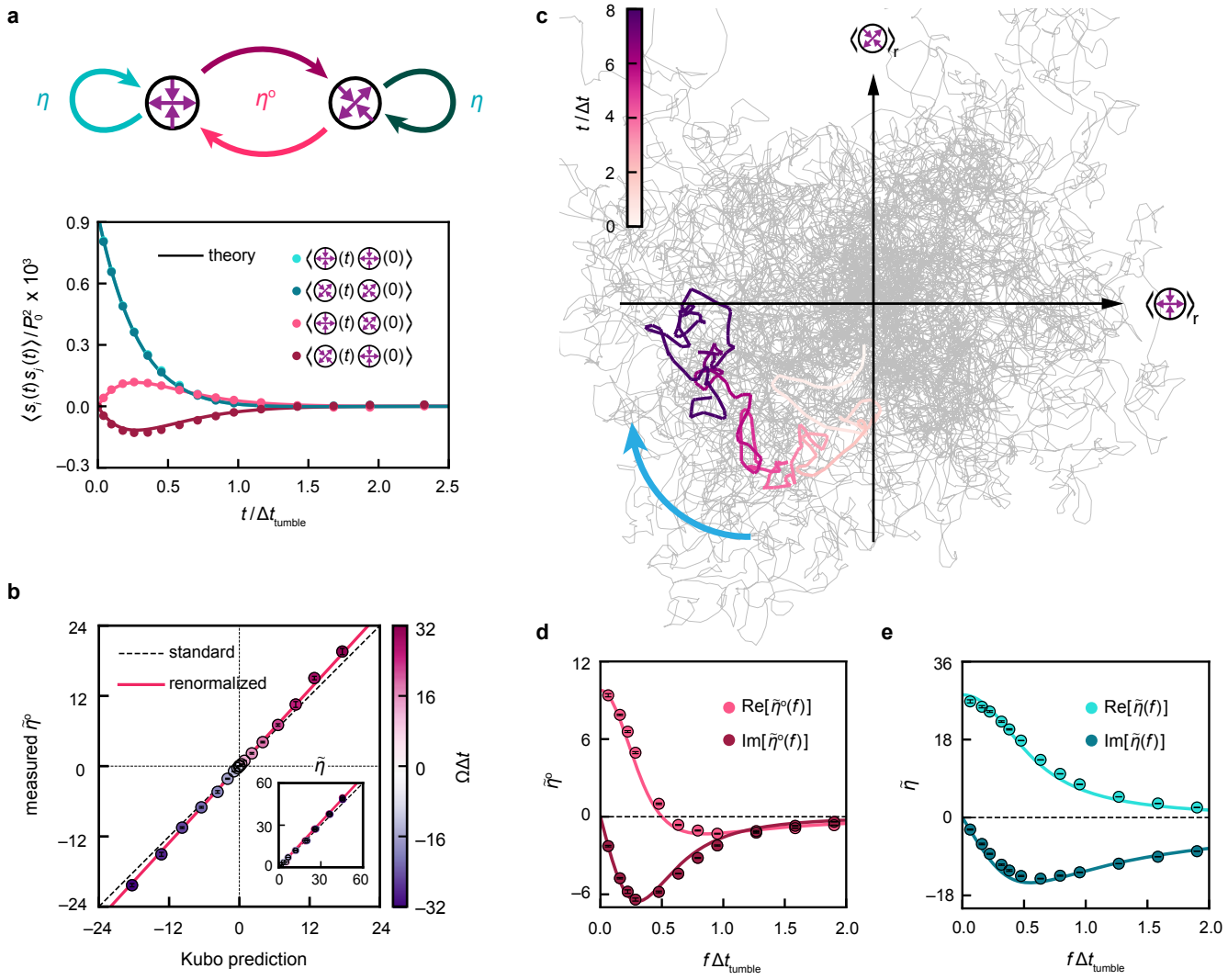

FIG. 4. **Green–Kubo relations and rheology in chiral active fluids. a.** Stress–stress correlation functions. The time correlation functions of the two global shear stresses $\langle \oplus \rangle_{\text{r}}$ and $\langle \otimes \rangle_{\text{r}}$ are plotted. The shear viscosity η leads to the auto-correlations (in green), whereas the odd viscosity η^{o} gives rise to the cross-correlations (in red), as summarized by the top schematic. The correlation functions predicted by our theory Eq. (13) are compared with the values measured in simulations. The correlation time is set by the tumbling time of a particle $\Delta t_{\text{tumble}} = (\Delta t + \Delta t_{\text{col}}) \cdot \bar{v}/\overline{\Delta v}$ required for a particle to randomize its direction, where Δt is the collision duration, Δt_{col} is the time between collisions, $\bar{v}$ is the mean velocity of the particle, and $\overline{\Delta v}$ is the average velocity change after a collision. We find that $\Delta t_{\text{tumble}} \approx 100 \Delta t$ in this case. **b.** Green–Kubo relation. The shear viscosities under constant shear are related to the integrated stress–stress correlations through the so-called direct-current (d.c.) Green–Kubo relation. The measured odd viscosity η^{o} is compared to the Green–Kubo prediction for a wide range of spinning speeds Ω. Inset: Comparison between the predicted and measured shear viscosity η. The Green–Kubo predictions with T_{eff} and the renormalized T^*_{eff} are marked as the dashed and solid lines, respectively. **c.** Time evolution of the shear stress vector $\left(\langle \oplus \rangle_{\text{r}}, \langle \otimes \rangle_{\text{r}}\right)$ at spinning speed $\Omega = 25.3/\Delta t$. At the steady state of the chiral active fluid, the shear stress vector traces out a 2D random walk in the stress space (grey curve in background), which is loosely confined and rotates around the origin preferentially in a clockwise fashion over time (curve with gradient coloring). **d-e.** Green–Kubo relation in frequency domain. The frequency-dependent coefficients of viscous response to an oscillatory shear with frequency f can be estimated using the Fourier transform of the stress–stress correlation functions. This is the so-called alternating-current (a.c.) Green–Kubo relation. Comparisons between the Green–Kubo predictions and the simulation measurements are presented for both odd viscosity (**d**) and shear viscosity (**e**) at various shear frequencies f. Error bars denote standard errors.

near $t = 0^{\pm}$ (see Supplementary Sec. VI), and $\langle\ \rangle$ denotes an ensemble average at the steady state. In standard fluctuating hydrodynamics [41, ch. IX], only the term proportional to $\delta(t)$ is included. Here, the second term has to be added to account for the effect of broken time-reversal invariance. The precise form of the functions $\delta(t)$ and $\xi(t)$ depends on the microscopic model. As shown in Fig. 3a,b (and Supplementary Sec. VI), the breaking of time-reversal invariance leads to qualitative changes in the stress correlations computed from molecular dynamics simulations: the imaginary parts of the correlation function in Fig. 3a would identically vanish in a time-reversal invariant system.

Experimentally, it is easier to access the velocity correlation functions

$$c_{ab}(\mathbf{r},t) = \big\langle u_a(\mathbf{r},t)u_b(0,0)\big\rangle \tag{10}$$

than the stress correlation functions. The Green function of the (linearized) Navier-Stokes equation Eq. (5) allows us to compute the velocity correlations Eq. (10) from the stress correlations Eq. (9), as we show in Supplementary Sec. VI. In Fig. 3c-f and Extended Fig. E5, we compare the correlations function directly obtained from the simulations with our theoretical predictions. In the hydrodynamic regime (wavevector $k \to 0$), there is an excellent agreement even when we assume no further information on the fluid than its viscosity coefficients. This corresponds to taking δ to the limit of a Dirac distribution (and similarly for ξ) in Eq. (9), see black curve in Fig. 3e. A discrepancy occurs at higher wavevectors, in which the microscopic time and length scales contained in the noise become relevant. A good agreement between Eq. (10) and the simulation results is recovered by using the measured stress correlations, see Fig. 3d and the red curve in Fig. 3e.

Green-Kubo relations

At equilibrium, correlation functions of the fluctuating stress yield the viscosities of a fluid. This relation known as the Green–Kubo formula is a manifestation of the fluctuation–dissipation theorem, whose validity is not guaranteed out of equilibrium [18, 19, 43–49].

Can the Green–Kubo relations survive in our active fluids? The answer is, in fact, already contained in the fluctuating hydrodynamic theory Eqs. (5–9). The Green–Kubo relations

$$\eta_{\alpha\beta} = \frac{A}{k_{\mathrm{B}}T_{\mathrm{eff}}}\int_0^\infty \big\langle \sigma^{\mathrm{R}}_\alpha(t)\sigma^{\mathrm{R}}_\beta(0)\big\rangle \mathrm{d}t \tag{11}$$

can be derived by integrating Eqs. (5–9) over space and time (A is the area of the 2D system). The second term in the right-hand side of Eq. (9), which is an antisymmetric function of time, yields the antisymmetric part of the viscosity matrix $\eta_{\alpha\beta}$ (containing e.g. the odd viscosity η^{o}). We numerically evaluate the right-hand side of Eq. (11) focusing on the two fluctuating shear stresses $s_1 = \oplus$ and $s_2 = \otimes$ (Fig. 4), and compare it with the viscosities obtained from linear response to finite perturbations. The auto-correlation function $\big\langle s_1(t)s_1(0)\big\rangle = \big\langle s_2(t)s_2(0)\big\rangle$ yields the shear viscosity η while the *cross*-correlation function $\big\langle s_1(t)s_2(0)\big\rangle = -\big\langle s_2(t)s_1(0)\big\rangle$ yields the odd viscosity η^{o} (Fig. 4a). The latter relation manifestly shows that $\eta^{\mathrm{o}} \neq 0$ violates time-reversal symmetry. As shown in Fig. 4b, the values of η and η^{o} computed from the Green–Kubo formula agree well with the values we obtained using the direct hydrodynamic measurements reported in Fig. 1. We verified that the long-time tails associated with the breakdown of 2D hydrodynamics are too small to impact the viscosity prediction (Supplementary Fig. S12).

In Supplementary Sec. VI, we derive both the fluctuating hydrodynamic Eqs. (5–9) and the Green–Kubo relations Eq. (11) from first principles, without invoking the Onsager regression hypothesis assumed in previous studies [31, 50]. By extending the Mori–Zwanzig projection operator formalism [51] to handle the presence of dissipative interactions, we derive the Green–Kubo relation and pinpoint the conditions of its validity. We show that an equilibrium-like Green–Kubo relation for the shear viscosity tensor holds near the steady-state of any isotropic active fluid satisfying the following three conditions: (i) the activated and fluctuating degrees of freedom are statistically decoupled; (ii) the steady state is stable under small perturbations; (iii) the ensemble-averaged (microscopic) velocity–velocity correlations $c_{\mathbf{vv}}(\mathbf{r}) = \big\langle \mathbf{v}(0)\cdot\mathbf{v}(\mathbf{r})\big\rangle$ (see Supplementary Figs. S13-S14) decay faster than r^{-D} (where D is the dimension of the system).

In order to take into account correlations between the particle velocities (see Methods Sec. C), the normalization factor $k_{\mathrm{B}}T_{\mathrm{eff}}$ in Eqs. (9) and (11) should in general be replaced with

$$k_{\mathrm{B}}T^*_{\mathrm{eff}} = k_{\mathrm{B}}T_{\mathrm{eff}} + \rho\,\hat{c}_{\mathbf{vv}}(\mathbf{k}\to 0)/D. \tag{12}$$

For our chiral active fluids with a contact frictional interaction, $c_{\mathbf{vv}}(\mathbf{r})$ is both small and local, causing a small but detectable correction that matches our predictions (red line in Fig. 4b). In wet active fluids, additional modifications of the Green-Kubo relation Eq. (11) are required because the hydrodynamic interactions can be non-reciprocal (see Supplementary Sec. VI).

Stress fluctuations and rheology

The behavior of the spatially averaged fluctuating shear stresses of a chiral active fluid can be understood visually from the following observation: the random trajectories of the collective variables $\langle\oplus\rangle_{\mathrm{r}}$ and $\langle\otimes\rangle_{\mathrm{r}}$ in shear-stress space plotted in Fig. 4c are random, confined, and have a tendency towards rotation (Supplementary Mov. S9). Here, $\langle\ \rangle_{\mathrm{r}}$ is an instantaneous spatial average (not the ensemble average $\langle\ \rangle$). To account for these properties, we introduce a minimal model based on the following Langevin equation (see discussions in Supple-

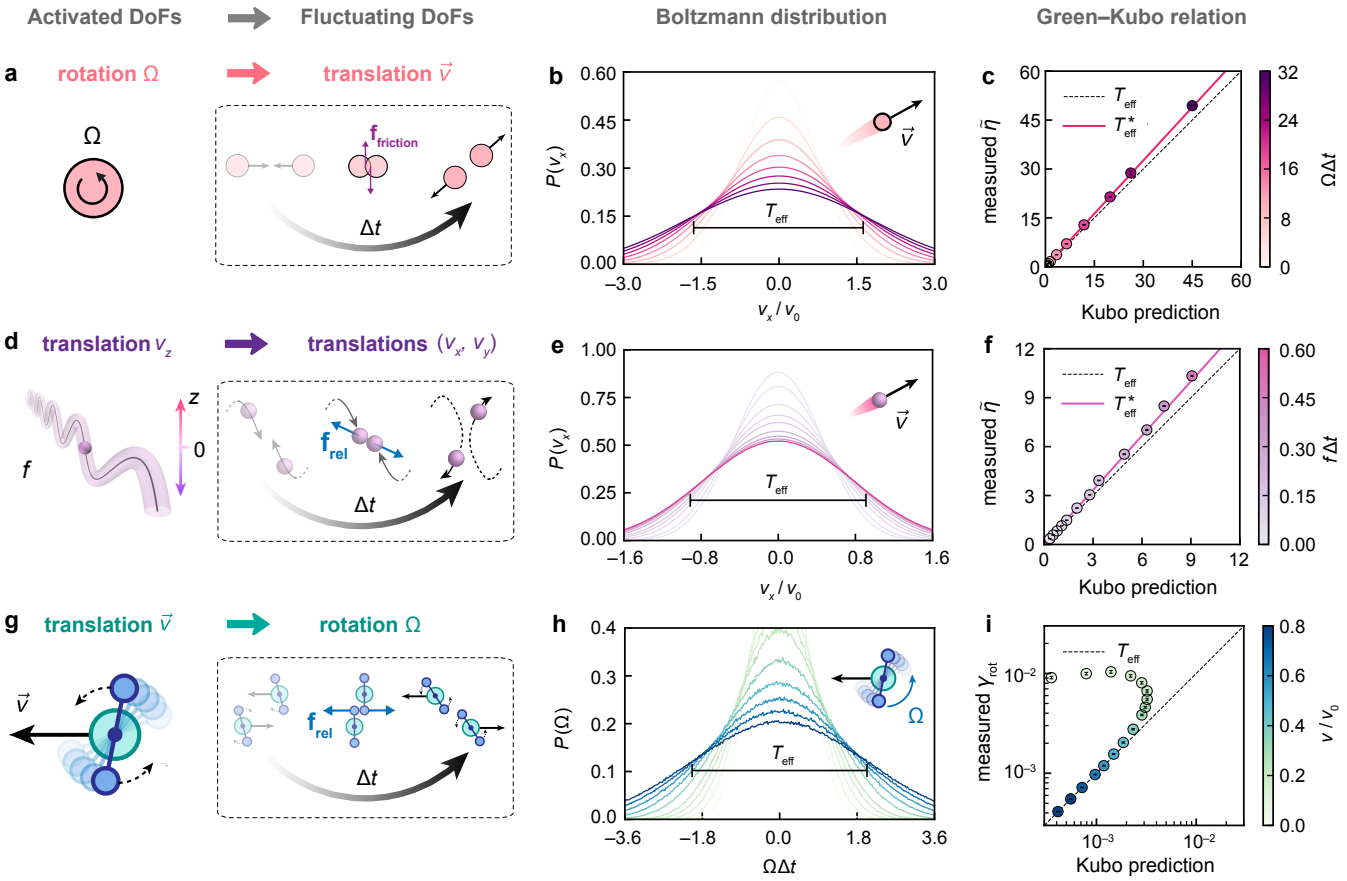

FIG. 5. **Effective thermodynamics in chiral active fluid, oscillating granular gas, and active Brownian rollers.** We consider three examples of active fluids in which the degrees of freedom are split into (i) activated degrees of freedom, directly powered by energy consumption, but whose dynamics reduces to a constraint on the relevant time scales, and (ii) fluctuating degrees of freedom that are powered through the activated ones (panels **a**,**d**,**g**). We find that the fluctuating degrees of freedom follow a Boltzmann distribution (**b**,**e**,**h**) and satisfy a Green–Kubo relation (**c**,**f**,**i**) when they are statistically decoupled from the activated degrees of freedom (see Fig. 6). **a-c.** Chiral active fluid. In this system, the active rotation of the particles powers their translational motion during collisions. The induced translational velocity displays a Boltzmann distribution parameterized by an effective temperature $T_{\rm eff} = m\langle v_x^2\rangle/k_{\rm B}$. The shear viscosity η satisfies the Green–Kubo relation associated with a renormalized temperature $T^*_{\rm eff}$, which quantifies the collective velocity fluctuations of a particle with its neighbors. **d-f.** Active oscillators. The particles oscillate in the z-direction at a constant frequency f with random initial phases. During collision, their vertical oscillation causes translations in the xy-plane. This induced horizontal translation displays a Boltzmann distribution as well as a Green–Kubo relation. See Extended Fig. E1 for more details. **g-i.** Active Brownian rollers. Active Brownian particles (green) hinged with a dumbbell (blue) self-propel at a constant speed v. During collision, this active translation causes a random rotation of the dumbbells, the angular velocity Ω of which follows a Boltzmann distribution. The rotational drag coefficient $\gamma_{\rm rot}$ measured via linear response follows a Green-Kubo relation at high activity v, but exhibits significant deviations from the Green-Kubo value at low activity v (see panel **i**). The damping coefficient $\gamma_{\rm rot}$ characterizes the relaxation of the rotation of individual particles (unlike the shear viscosity η that describe the relaxation of collective hydrodynamic variables). Hence, the effective temperature $T_{\rm eff} = I\langle\Omega^2\rangle/2k_{\rm B}$ (where I is the moment of inertia) entering the Green–Kubo relation includes no correction from correlations (contrary to the two other systems in which the renormalized temperature $T^*_{\rm eff}$ appears). See Extended Fig. E2 for more details. We have defined $v_0 = d/\Delta t$. The number density is $nd^2 = 0.254$ in both chiral active fluid and oscillating granular gas, whereas $nd^2 = 0.076$ in the system of active Brownian rollers. Error bars denote standard errors.

mentary Sec. VII and Fig. S18)

$$\begin{pmatrix} \dot{\langle \circledast \rangle_{\mathrm{r}}} \\ \dot{\langle \circledcirc \rangle_{\mathrm{r}}} \end{pmatrix} = -C_{\boldsymbol{\eta}} \begin{pmatrix} \eta & \eta^{\mathrm{o}} \\ -\eta^{\mathrm{o}} & \eta \end{pmatrix}^{-1} \begin{pmatrix} \langle \circledast \rangle_{\mathrm{r}} \\ \langle \circledcirc \rangle_{\mathrm{r}} \end{pmatrix} + C_{\mathbf{R}} \begin{pmatrix} w_1 \\ w_2 \end{pmatrix}, \qquad (13)$$

where w_1 and w_2 are two independent white noise components, the prefactors $C_{\boldsymbol{\eta}} = \left\langle \langle \circledast \rangle_{\mathrm{r}}^2(0) \right\rangle A/k_{\mathrm{B}}T^*_{\mathrm{eff}}$ and $C_{\mathbf{R}} = \left\langle \langle \circledast \rangle_{\mathrm{r}}^2(0) \right\rangle \sqrt{A/k_{\mathrm{B}}T^*_{\mathrm{eff}} \cdot \eta/(\eta^2+\eta^{\mathrm{o}2})}$. When the odd viscosity η^{o} vanishes, Eq. (13) simply describes the evolution of an overdamped random walker with Cartesian coordinates $(\langle \circledast \rangle_{\mathrm{r}}, \langle \circledcirc \rangle_{\mathrm{r}})$ moving in a harmonic trap. In the presence of a non-vanishing η^{o}, the random walker experiences an additional azimuthal force proportional to its distance from the origin that makes it rotate as shown in Fig. 4c. (This is formally equivalent to the odd elastic springs of Ref. [23] with addition of a random noise.) This chiral motion again shows the breaking of time-reversal symmetry caused by η^{o}.

In Supplementary Sec. VII, we solve Eq. (13) analytically and find closed-form expressions for the stress–stress correlation functions (plotted as continuous lines in Fig. 4a) that match well with the molecular dynamics simulation measurements (plotted as dots in Fig. 4a). By Fourier transforming these analytically derived correlation functions, we can predict the viscous response to an oscillatory shear with frequency f. The complex shear viscosity $\eta(f) = \eta'(f) - \mathrm{i}\eta''(f)$ is related to the dynamic (complex) shear modulus $G(f) = G'(f) + \mathrm{i}G''(f)$ through $\eta' = G''/[2\pi f]$ and $\eta'' = G'/[2\pi f]$ [25]. Here, G' is the storage modulus describing the elastic response and G'' is the loss modulus describing the viscous response. Similarly, a complex odd viscosity $\eta^o(f) = \eta^{o\prime}(f) - \mathrm{i}\eta^{o\prime\prime}(f)$ can be related to an odd dynamic modulus $G^o(f) = \eta^o(f)/[2\pi \mathrm{i} f]$. See also Ref. [26] for a discussion of odd viscoelastic materials. As illustrated in Fig. 4d-e, the predicted $\eta(f)$ and $\eta^{\mathrm{o}}(f)$ are in excellent agreement with numerical data. This provides a finite-frequency extension of the Green–Kubo formula.

Statistical decoupling and mutual information

Is the presence of an equilibrium-like Green-Kubo relation restricted to chiral active fluids? To investigate this question, we performed extensive simulations of active Brownian rollers and oscillating granular gases (Fig. 5). In both cases, the non-equilibrium steady-state follows an approximate Boltzmann distribution (Fig. 5e and Fig. 5h), parametrized by an effective temperature T_{eff} controlled by the respective sources of activity. In addition, Fig. 5f,i shows that a Green–Kubo relation also applies to the shear viscosity of oscillating granular gases and the drag coefficient of active Brownian rollers with the same T_{eff} values measured in Fig. 5e,h.

We trace the validity of the Green–Kubo relation in all these systems to the statistical decoupling between activated and fluctuating degrees of freedom. Energy is passed from the environment to the fluctuating degrees of freedom through the activated ones. Yet, the activated and fluctuating degrees of freedom can still be almost statistically independent. This is evidenced by Fig. 6, in which we plot the mutual information between the activated and fluctuating degrees of freedom, defined as the Kullback-Leibler divergence [52]

$$I^{(\mathrm{a,f})} = \int P(X^{\mathrm{a}}, X^{\mathrm{f}}) \ln \left[\frac{P(X^{\mathrm{a}}, X^{\mathrm{f}})}{P(X^{\mathrm{a}})\, P(X^{\mathrm{f}})} \right] \mathrm{d}X^{\mathrm{a}} \mathrm{d}X^{\mathrm{f}} \qquad (14)$$

between the post-collision joint distribution of the random variables X^{a} and X^{f} associated with the activated and fluctuating degrees of freedom and the products of their marginal distributions (see Supplementary Sec. VIII). To allow comparison between different systems, we normalize the mutual information $I^{(\mathrm{a,f})}$ by the joint entropy $H^{(\mathrm{a,f})}$ between X^{a} and X^{f}. The factorisation of the joint distributions (or lack thereof) is illustrated in Fig. 6. Crucially, the deviation from the Green-Kubo relation for active Brownian rollers in Fig. 6j coincides with a sharp increase of the mutual information. The Green–Kubo formula for the fluctuating rotational degrees of freedom is valid in the limit of large self-propulsion speed (or high drag coefficient; see Extended Fig. E2c-d, respectively), where the drive wipes out most correlations with the activated translational degrees of freedom. In contrast, the mutual information is approximately constant in Fig. 6b,f. Here, the Green-Kubo relation is always valid for the range of parameters we explored.

Our fluctuating hydrodynamic theory of active fluids offers a probe of their anomalous transport coefficients and paves the way for studies of chiral active turbulence.

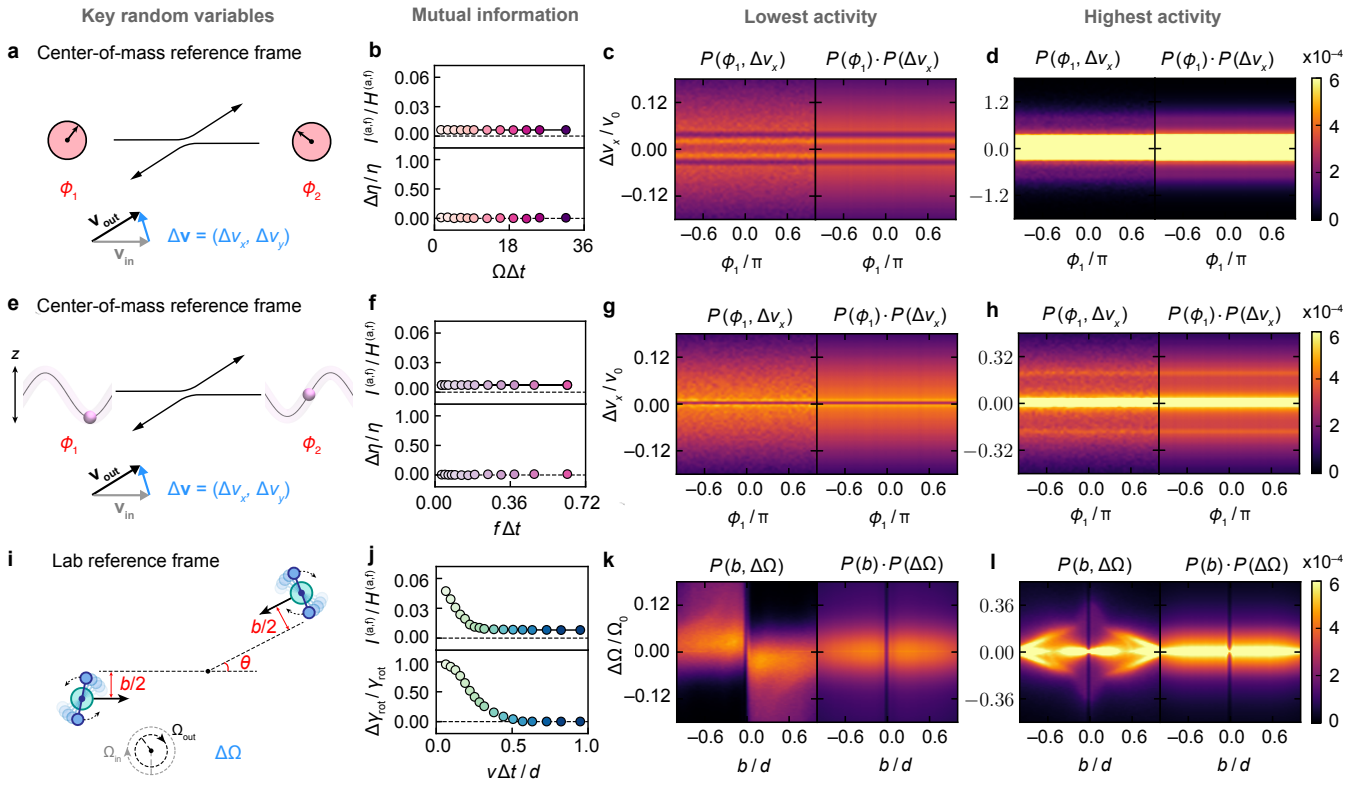

FIG. 6. **Mutual information in chiral active fluid, oscillating granular gases, and active Brownian rollers.** We quantify the statistical interdependence between the activated and fluctuating degrees of freedom (DoFs) during collision, by computing the mutual information $I^{(\mathrm{a,f})}$ (defined in Eq. (14)) between them. We first identify the key random variables for the activated and fluctuating DoFs during collision, which are marked in red and blue, respectively, in panels **a**,**e**,**i**. By performing simulations of scattering events, we then sample the joint probability distributions of those random variables, which allows us to further calculate $I^{(\mathrm{a,f})}$. In panels **b**,**f**,**j**, we compare the mutual information $I^{(\mathrm{a,f})}$ normalized by joint entropy $H^{(\mathrm{a,f})}$ and the deviation from the Green–Kubo relation for a wide range of activity. **a-d.** Chiral active fluid. We select the initial orientation of the two spinners (ϕ_1, ϕ_2) as the random variables for active rotations, while the velocity change upon collision $\Delta\mathbf{v} = (\Delta v_x, \Delta v_y)$ as the random variable for fluctuating translations, see panel **a**. Due to the isotropic nature of the spinners, collision should not depend on particle orientations. Indeed, the normalized mutual information $I^{(\mathrm{a,f})}/H^{(\mathrm{a,f})}$ between (ϕ_1, ϕ_2) and $(\Delta v_x, \Delta v_y)$ is negligible, suggesting that the activated and fluctuating DoFs are statistically decoupled, see panel **b**. The small nonzero residue in $I^{(\mathrm{a,f})}/H^{(\mathrm{a,f})}$ is caused by the noise in the probability distribution sampled from simulations. Consistently, the relative difference between the measured shear viscosity and the Kubo prediction, $\Delta\eta/\eta = (\eta - \eta_{\mathrm{Kubo}})/\eta$, is negligible. To further demonstrate the statistical independence, we plot the joint distribution $P(\phi_1, \Delta v_x)$ in **c** and the products of marginal distributions $P(\phi_1)P(\Delta v_x)$ in **d** at both the lowest and highest activities (first and last points in panel **b**). The results show that the probability distribution of the activated and fluctuating DoFs can indeed be factorized. **e-h.** Active oscillators. Here we select the initial phases of the two oscillators (ϕ_1, ϕ_2) and the velocity change $\Delta\mathbf{v} = (\Delta v_x, \Delta v_y)$ as the key random variables. Our results show these activated and fluctuating DoFs are also statistically decoupled. **i-l.** Active Brownian rollers. We select the impact parameter b and the incident angle θ as the random variables for active translations and the change in the rotation velocity $\Delta\Omega$ as the key random variable for the linear response in fluctuating rotations. The normalized mutual information $I^{(\mathrm{a,f})}/H^{(\mathrm{a,f})}$ and the deviation from the Kubo relation quantified as $\Delta\gamma_{\mathrm{rot}}/\gamma_{\mathrm{rot}} = (\gamma_{\mathrm{rot}} - \gamma_{\mathrm{rot\text{-}Kubo}})/\gamma_{\mathrm{rot}}$ simultaneously decrease with activity, see panel **j**.

[1] L. P. Kadanoff, "Built upon sand: Theoretical ideas inspired by granular flows," Rev. Mod. Phys. **71**, 435–444 (1999).

[2] P. G. de Gennes, "Granular matter: a tentative view," Rev. Mod. Phys. **71**, S374–S382 (1999).

[3] H. M. Jaeger, S. R. Nagel, and R. P. Behringer, "Granular solids, liquids, and gases," Rev. Mod. Phys. **68**, 1259–1273 (1996).

[4] B. A. Grzybowski, H. A. Stone, and G. M. Whitesides, "Dynamic self-assembly of magnetized, millimetre-sized objects rotating at a liquid-air interface," Nature **405**, 1033–1036 (2000).

[5] J.-C. Tsai, F. Ye, J. Rodriguez, J. P. Gollub, and T. Lubensky, "A chiral granular gas," Phys. Rev. Lett. **94**, 214301 (2005).

[6] S. Fürthauer, M. Strempel, S. W. Grill, and F. Jülicher, "Active chiral fluids," Eur. Phys. J. E **35**, 1–13 (2012).

[7] N. H. Nguyen, D. Klotsa, M. Engel, and S. C. Glotzer, "Emergent collective phenomena in a mixture of hard shapes through active rotation," Phys. Rev. Lett. **112**, 075701 (2014).

[8] B. C. van Zuiden, J. Paulose, W. T. M. Irvine, D. Bartolo, and V. Vitelli, "Spatiotemporal order and emergent edge currents in active spinner materials," Proc. Natl. Acad. Sci. U.S.A. **113**, 12919–12924 (2016).

[9] D. Banerjee, A. Souslov, A. G. Abanov, and V. Vitelli, "Odd viscosity in chiral active fluids," Nat. Commun. **8**, 1573 (2017).

[10] C. Scholz, M. Engel, and T. Pöschel, "Rotating robots move collectively and self-organize," Nat. Commun. **9**, 931 (2018).

[11] V. Soni, E. S. Bililign, S. Magkiriadou, S. Sacanna, D. Bartolo, M. J. Shelley, and W. T. M. Irvine, "The odd free surface flows of a colloidal chiral fluid," Nat. Phys. **15**, 1188–1194 (2019).

[12] K. Yeo, E. Lushi, and P. M. Vlahovska, "Collective dynamics in a binary mixture of hydrodynamically coupled microrotors," Phys. Rev. Lett. **114**, 188301 (2015).

[13] T. Markovich, E. Tjhung, and M. E. Cates, "Chiral active matter: microscopic 'torque dipoles' have more than one hydrodynamic description," New J. Phys. **21**, 112001 (2019).

[14] N. Oppenheimer, D. B. Stein, and M. J. Shelley, "Rotating membrane inclusions crystallize through hydrodynamic and steric interactions," Phys. Rev. Lett. **123**, 148101 (2019).

[15] I. H. Riedel, K. Kruse, and J. Howard, "A self-organized vortex array of hydrodynamically entrained sperm cells," Science **309**, 300–303 (2005).

[16] A. P. Petroff, X.-L. Wu, and A. Libchaber, "Fast-moving bacteria self-organize into active two-dimensional crystals of rotating cells," Phys. Rev. Lett. **114**, 158102 (2015).

[17] F. Rouyer and N. Menon, "Velocity fluctuations in a homogeneous 2d granular gas in steady state," Phys. Rev. Lett. **85**, 3676–3679 (2000).

[18] G. D'Anna, P. Mayor, A. Barrat, V. Loreto, and F. Nori, "Observing brownian motion in vibration-fluidized granular matter," Nature **424**, 909–912 (2003).

[19] R. Ojha, P.-A. Lemieux, P. Dixon, A. Liu, and D. Durian, "Statistical mechanics of a gas-fluidized particle," Nature **427**, 521 (2004).

[20] P. Romanczuk, M. Bär, W. Ebeling, B. Lindner, and L. Schimansky-Geier, "Active brownian particles," Eur. Phys. J.: Spec. Top. **202**, 1–162 (2012).

[21] M. E. Cates and J. Tailleur, "Motility-induced phase separation," Annu. Rev. Condens. Matter Phys. **6**, 219–244 (2015).

[22] S. Luding, "Cohesive, frictional powders: contact models for tension," Granul. Matter **10**, 235–246 (2008).

[23] C. Scheibner, A. Souslov, D. Banerjee, P. Surówka, W. T. M. Irvine, and V. Vitelli, "Odd elasticity," Nat. Phys. **16**, 475–480 (2020).

[24] J. Avron, "Odd viscosity," J. Stat. Phys. **92**, 543–557 (1998).

[25] P. Oswald, *Rheophysics - The Deformation And Flow Of Matter* (Cambridge University Press, 2014).

[26] D. Banerjee, V. Vitelli, F. Jülicher, and P. Surówka, "Active viscoelasticity of odd materials," Phys. Rev. Lett. **126**, 138001 (2021).

[27] J. Irving and J. G. Kirkwood, "The statistical mechanical theory of transport processes. iv. the equations of hydrodynamics," J. Chem. Phys. **18**, 817–829 (1950).

[28] D. W. Condiff and J. S. Dahler, "Fluid mechanical aspects of antisymmetric stress," Phys. Fluids **7**, 842 (1964).

[29] D. J. Evans and G. Morriss, *Statistical mechanics of nonequilibrium liquids* (Cambridge University Press, 2008).

[30] A. Souslov, K. Dasbiswas, M. Fruchart, S. Vaikuntanathan, and V. Vitelli, "Topological waves in fluids with odd viscosity," Phys. Rev. Lett. **122**, 128001 (2019).

[31] J. M. Epstein and K. K. Mandadapu, "Time reversal symmetry breaking in two-dimensional non-equilibrium viscous fluids," arXiv preprint arXiv:1907.10041 (2019).

[32] J. Korving, H. Hulsman, H. Knaap, and J. Beenakker, "Transverse momentum transport in viscous flow of diatomic gases in a magnetic field," Phys. Lett. **21**, 5–7 (1966).

[33] P. Wiegmann and A. G. Abanov, "Anomalous hydrodynamics of two-dimensional vortex fluids," Phys. Rev. Lett. **113**, 034501 (2014).

[34] T. Markovich and T. C. Lubensky, "Odd viscosity in active matter: microscopic origin and 3d effects," arXiv preprint arXiv:2006.05662 (2020).

[35] A. I. Berdyugin, S. Xu, F. Pellegrino, R. K. Kumar, A. Principi, I. Torre, M. B. Shalom, T. Taniguchi, K. Watanabe, I. Grigorieva, *et al.*, "Measuring hall viscosity of graphene's electron fluid," Science **364**, 162–165 (2019).

[36] B. Bradlyn, M. Goldstein, and N. Read, "Kubo formulas for viscosity: Hall viscosity, ward identities, and the relation with conductivity," Phys. Rev. B **86**, 245309 (2012).

[37] C. Hoyos and D. T. Son, "Hall viscosity and electromagnetic response," Phys. Rev. Lett. **108**, 066805 (2012).

[38] S. R. De Groot and P. Mazur, *Non-equilibrium thermodynamics* (Courier Corporation, 2013).

[39] H. B. G. Casimir, "On onsager's principle of microscopic reversibility," Rev. Mod. Phys. **17**, 343 (1945).

[40] U. Geigenmüller, U. Titulaer, and B. Felderhof, "The approximate nature of the onsager-casimir reciprocal relations," Phys. A: Stat. Mech. Appl. **119**, 53–66 (1983).

[41] L. Landau, E. Lifšic, E. Lifshitz, L. P, L. Pitaevskii, J. Sykes, and M. Kearsley, *Statistical Physics, Part 2: Theory of the Condensed State*, Course of theoretical physics, Vol. 9 (Elsevier Science, 1980).

[42] J. M. O. de Zarate and J. V. Sengers, *Hydrodynamic Fluctuations In Fluids And Fluid Mixtures* (Elsevier, 2006).

[43] J. Kurchan, "In and out of equilibrium," Nature **433**, 222–225 (2005).

[44] S. Ciliberto, S. Joubaud, and A. Petrosyan, "Fluctuations in out-of-equilibrium systems: from theory to experiment," J. Stat. Mech.: Theory Exp. **2010**, P12003 (2010).

[45] L. F. Cugliandolo, "The effective temperature," Journal of Physics A: Mathematical and Theoretical **44**, 483001 (2011).

[46] D. Loi, S. Mossa, and L. F. Cugliandolo, "Effective temperature of active matter," Phys. Rev. E **77**, 051111 (2008).

[47] U. Seifert, "Stochastic thermodynamics, fluctuation theorems and molecular machines," Rep. Prog. Phys. **75**, 126001 (2012).

[48] Y. Shokef, G. Bunin, and D. Levine, "Fluctuation-dissipation relations in driven dissipative systems," Phys. Rev. E **73**, 046132 (2006).

[49] H. A. Makse and J. Kurchan, "Testing the thermodynamic approach to granular matter with a numerical model of a decisive experiment," Nature **415**, 614–617 (2002).

[50] R. Kubo, M. Yokota, and S. Nakajima, "Statistical-mechanical theory of irreversible processes. II. response to thermal disturbance," J. Phys. Soc. Japan. **12**, 1203–1211 (1957).

[51] R. Zwanzig, *Nonequilibrium Statistical Mechanics*, 3rd ed. (Oxford University Press, 2001).

[52] D. J. C. MacKay, *Information Theory, Inference And Learning Algorithms* (Cambridge University Press, 2003).

METHODS

A. Models and simulations

1. Chiral active fluid

We study the behavior of a quasi-2D chiral active fluid composed of spinning components [5–7, 10, 13, 16, 53–56]. The microscopic model is presented in the main text (Eqs. (1) and (2)). This model is adapted from standard models of frictional granular disks, see Ref. [22] as well as the documentation of the LAMMPS package [57, 58] (`pair_granular`) and references therein. Compared to these standard granular models [22, 57, 58], here we have made the following simplifications: (i) rolling friction is ignored; (ii) the frictional coefficients in the normal (radial) and tangential directions take the same value γ.

To prevent complete interpenetration between the particles, we add a nonlinearity to the repulsion $\mathbf{f}^{\mathrm{c}}$, with a distance-dependent Hookean coefficient that diverges at $r_{ij} = 0$:

$$k(r_{ij}) = k\left(1 + \alpha \frac{\mathrm{d}}{r_{ij}}\right). \tag{M.1}$$

Regarding $\mathbf{f}_{ij}^{\mathrm{nc}}$ in Eq. (3), we emphasize that this interaction is not central, and not invariant under spatial transformations that change orientation (such as reflections). Hence, this granular gas is an example of a broader class of systems called parity-violating fluids [9, 24, 37] that includes driven granular gases [5, 8], rotating colloids [11, 12, 59–61], polyatomic gases in magnetic fields [32], vortex fluids [33], and electronic fluids [35, 36].

The model defined by Eqs. (1) and (2) is analyzed through particle-based simulations using a customized version of the LAMMPS package [57, 58]. We choose the area fraction of the system to be $\phi = 0.2$ and set $\gamma_{\mathrm{rot}} = 3md^2/t_0$, $\gamma = 0.015m/t_0$, $k = m/t_0^2$, and $\alpha = 0.3$, where m is the particle mass and t_0 is the unit of time of the simulation and d is the unit of length of the simulation. The interaction timescale $\Delta t = \sqrt{m/k}$ is then $\Delta t = t_0$. To focus on the viscous effects emergent from particle interactions, a frictionless background is used. All the simulations are initialized with a random velocity distribution. The results are collected after the system reaches a steady state. In Supplementary Sec. I, we detail specific procedures for investigating the effective thermodynamics [43, 45, 46, 59, 62–66] (including antisymmetric stress [28, 67–71]), kinetics, linear response, Green–Kubo relation [43, 44, 47, 63, 66, 72–82] and hydrodynamics.

2. Active oscillators

Consider a quasi-2D granular gas composed of the same particles as the chiral fluid of Methods Sec. A 1. Instead of self-spinning, all the particles oscillate in the z-direction at a constant frequency f. In particular, each particle is driven to move in the range $z \in [-A, A]$ with a target velocity profile

$$v_0(t) = 2\pi\omega A \sin(\omega t + \phi), \tag{M.2}$$

where $\omega = 2\pi f$ is the angular frequency and ϕ is a random initial phase of the oscillation. To ensure all particles roughly stay in the same horizontal plane ($z = 0$), a linear restoring force $\mathbf{f} = -k_z z\,\hat{\mathbf{z}}$ is added. The microscopic dynamics of the system can be summarized as

$$m\ddot{x}_i = \sum_{j\in N(i)} f_{ij,x}, \tag{M.3}$$

$$m\ddot{y}_i = \sum_{j\in N(i)} f_{ij,y}, \tag{M.4}$$

$$m\ddot{z}_i = c_{\mathrm{d}}\big[v_{i,0}(t) - v_{i,z}\big] - k_z z + \sum_{j\in N(i)} f_{ij,z}, \tag{M.5}$$

where c_{d} is a large drag coefficient that forces the particle velocity $v_{i,z}$ to quickly relax to $v_{i,0}(t)$. The conservative part of the interaction $\mathbf{f}_{ij}^{\mathrm{c}}$ is the same as before, see Eq. (3). The dissipative interaction here takes the form:

$$\mathbf{f}_{ij}^{\mathrm{nc}} = \begin{cases} -\gamma \mathbf{v}_{ij}, & r_{ij} < d, \\ 0 & r_{ij} \geq d. \end{cases} \tag{M.6}$$

Upon collision, the z-directional oscillations of the particles induce random motions in the xy-plane.

All the simulations are performed at an area fraction $\phi = 0.2$. We set the parameters $A = d$ and $c_d = 100m/t_0$ for the oscillation, $\gamma = 0.015m/t_0$, $k = m/t_0^2$ and $\alpha = 0.3$ for particle interaction.

To confirm the Boltzmann statistics, we measure the probability distribution of the induced horizontal velocity at various oscillating frequencies $f \in [0.03/\Delta t, 0.6/\Delta t]$. We measure the effective temperature as $T_{\mathrm{eff}} = m\langle v_x^2\rangle / k_{\mathrm{B}}$. In addition, we also measure the density profile of the system when exposed to an external potential well of magnitude $-0.5k_{\mathrm{B}}T_{\mathrm{eff}}$.

Lastly, we study the Green–Kubo relation for the shear viscosity (Eq. (11) with $\alpha = \beta = 2$ or 3, see Sec. B for the notations) for $f \in [0.03/\Delta t, 0.6/\Delta t]$, by comparing the value directly measured from linear response under shear flow with the Kubo prediction at the steady state. The detailed procedure is identical to the one described for the chiral active fluid in Supplementary Sec. I.

3. Active Brownian rollers

Consider a 2D system composed of active Brownian rollers. Each roller contains a core particle of mass m_{c} and diameter d_{c} as well as two dumbbell particles of mass m_{r} and diameter d_{r}, which are away from the roller center by s, hinged to the core particle by a rigid bond and free to rotate about it, see Fig. E2. The core particle self-propels at a constant speed v in its own orientation $\hat{\mathbf{e}} =$

$\big(\cos\theta, \sin\theta\big)$, where θ is the tilt angle of the orientation director against the x-axis. The excluded-volume effects of both the core and dumbbell particles are modeled by the conservative interaction $\mathbf{f}_{ij}^{\mathrm{c}}$ in Eq. (3). However, no dissipative interaction is included. During collision, the self-propulsion of two active Brownian rollers could cause random rotation of their dumbbells, which is quantified by the rotation speed Ω. The microscopic dynamics of the system is described as

$$m_{\mathrm{c}}\ddot{\mathbf{x}}_i = c_{\mathrm{d}}\big[v\hat{\mathbf{e}}_i - \mathbf{v}_i\big] + \sum_{j\in N(i)} \mathbf{f}_{ij} + \boldsymbol{\xi}_{\mathbf{x}}(t) \tag{M.7}$$

$$I_{\mathrm{c}}\ddot{\theta}_i = -\Gamma_{\mathrm{c}}\dot{\theta}_i + \xi_\theta(t) \tag{M.8}$$

$$I_{\mathrm{r}}\dot{\Omega}_i = \sum_{j\in N(i)} \boldsymbol{\tau}_{ij} \tag{M.9}$$

where c_{d} and Γ_{c} are the translational and rotational drag coefficients for the core particle, $\boldsymbol{\xi}_{\mathbf{x}}(t)$ is the white noise for translational motion satisfying $\langle \xi_{\mathbf{x},a}(t)\xi_{\mathbf{x},b}(t')\rangle = 2c_{\mathrm{d}}k_{\mathrm{B}}T_{\mathbf{x}}\delta(t-t')$, $\xi_\theta(t)$ is the white noise for the reorientation of the director $\hat{\mathbf{e}}$ satisfying $\langle \xi_\theta(t)\xi_\theta(t')\rangle = 2\Gamma_{\mathrm{c}}k_{\mathrm{B}}T_\theta\delta(t-t')$, and I_{c} and I_{r} are the moments of inertia for the core and dumbbell particles, respectively. $\boldsymbol{\tau}_{ij}$ is the total torque exerted on the dumbbell of particle i by particle j, as a consequence of both the core–dumbbell and dumbbell–dumbbell interactions. These interparticle collisions lead to an effective drag coefficient γ_{rot} for the rotation of the dumbbell.

All the simulations are performed at an area fraction $\phi = 0.06$. We set the parameters $m_{\mathrm{c}} = m$, $d_{\mathrm{c}} = d$, and $I_{\mathrm{c}} = 0.1md^2$ for the core particle, $d_{\mathrm{r}} = 0.2d$, $m_{\mathrm{r}} = m$, $I_{\mathrm{r}} = 0.728md^2$, $s = 0.6d$ for the dumbbell, $c_{\mathrm{d}} = 100m/t_0$ and $k_{\mathrm{B}}T_{\mathbf{x}} = 0$ for active translation, $\Gamma_{\mathrm{c}} = c_{\mathrm{d}}d^2$ and $k_{\mathrm{B}}T_\theta = 10^{-3}md^2/t_0^2$ for the director reorientation, and lastly $k = m/t_0^2$, and $\alpha = 0.3$ for particle interactions.

To validate the Boltzmann statistics, we measure the probability distribution of the dumbbell rotation speed Ω at various self-propulsion speed $v \in [0.06d/\Delta t,\ 0.8d/\Delta t]$. From the measured probability distribution $P(\Omega)$, we can quantify the effective temperature $T_{\mathrm{eff}} = I_{\mathrm{r}}\langle\Omega^2\rangle/k_{\mathrm{B}}$.

We also study the Green–Kubo relation of the effective rotational drag coefficient γ_{rot} for a wide range of self-propulsion speed $v \in [0.06d/\Delta t,\ 0.8d/\Delta t]$ at a constant $c_{\mathrm{d}} = 100md/\Delta t$ as well as a wide range of drag coefficient $c_{\mathrm{d}} \in [0.1md/\Delta t, 10^3md/\Delta t]$ at a constant $v = 0.3d/\Delta t$. In particular, we directly measure γ_{rot} by investigating the linear response of single-particle rotation towards a small external torque $\tau_{\mathrm{ext}} \in [10^{-4}md^2/\Delta t^2, 10^{-3}md^2/\Delta t^2]$, and further compared it with the Kubo prediction

$$\gamma_{\mathrm{rot}} = \frac{1}{k_{\mathrm{B}}T_{\mathrm{eff}}}\int_0^\infty \langle\tau(t)\tau(0)\rangle\,\mathrm{d}t, \tag{M.10}$$

where $\tau(t)$ is the fluctuating random torque experienced by a given particle due to collision with its neighbors at the steady state.

B. Viscosity: notations and symmetry considerations

In this section, we introduce the notation used in Eq. (6) of the main text and discuss how various physical symmetries restrict the form of the viscosity tensor. The viscous stress tensor is linearly related to velocity gradients by the viscosity tensor through the equation

$$\sigma_{ab}^{\mathrm{vis}} = \eta_{abcd}\,\dot{e}_{cd} \tag{M.11}$$

where $\sigma_{ab}^{\mathrm{vis}}$ is the viscous stress tensor, $\dot{e}_{cd} = \partial_d u_c$ is the (unsymmetrized) velocity gradient tensor, and η_{abcd} is the viscosity tensor.

Following Refs. [23, 24], we introduce the following basis for rank-2 tensors in two dimensions:

$$\begin{aligned} \tau_{ab}^0 &= \begin{pmatrix} 1 & 0 \\ 0 & 1 \end{pmatrix} & \tau_{ab}^1 &= \begin{pmatrix} 0 & -1 \\ 1 & 0 \end{pmatrix} \\ \tau_{ab}^2 &= \begin{pmatrix} 1 & 0 \\ 0 & -1 \end{pmatrix} & \tau_{ab}^3 &= \begin{pmatrix} 0 & 1 \\ 1 & 0 \end{pmatrix}. \end{aligned} \tag{M.12}$$

These are irreducible tensors with respect to the orthogonal group $O(2)$. More precisely, we consider the representation of $O(2)$ on rank-2 tensors (by which a tensor T_{ab} is transformed into $g_{aa'}\,g_{bb'}\,T_{a'b'}$ for $g \in O(2)$) and decompose it in irreducible representations (IRs): two 1D IRs (scalar, corresponding to the basis tensor τ^0; and pseudoscalar, corresponding to τ^1) and a 2D IR (with basis tensors τ^2 and τ^3). (See e.g. Ref. [83, p. 376] for the IR of O(2). With the notations of this reference, we have used $r^1 \times r^1 \simeq \varphi^1 + \varphi^2 + r^2$.)

We use the τ_{ab}^α to decompose the stress and velocity gradient tensors into irreducible components via the following definitions:

$$\oplus \triangleq \frac{1}{2}\tau_{ab}^0\sigma_{ab} = (\sigma_{xx} + \sigma_{yy})/2 \tag{M.13a}$$

$$\circlearrowright \triangleq \frac{1}{2}\tau_{ab}^1\sigma_{ab} = (\sigma_{yx} - \sigma_{xy})/2 \tag{M.13b}$$

$$\oplus \triangleq \frac{1}{2}\tau_{ab}^2\sigma_{ab} = (\sigma_{xx} - \sigma_{yy})/2 \tag{M.13c}$$

$$\otimes \triangleq \frac{1}{2}\tau_{ab}^3\sigma_{ab} = (\sigma_{xy} + \sigma_{yx})/2 \tag{M.13d}$$

and

$$\dot{\square} \triangleq \tau_{ab}^0\dot{e}_{ab} = \dot{e}_{xx} + \dot{e}_{yy} \tag{M.14a}$$

$$\dot{\diamond} \triangleq \tau_{ab}^1\dot{e}_{ab} = \dot{e}_{yx} - \dot{e}_{xy} \tag{M.14b}$$

$$\dot{\square} \triangleq \tau_{ab}^2\dot{e}_{ab} = \dot{e}_{xx} - \dot{e}_{yy} \tag{M.14c}$$

$$\dot{\diamond} \triangleq \tau_{ab}^3\dot{e}_{ab} = \dot{e}_{xy} + \dot{e}_{yx}. \tag{M.14d}$$

Furthermore, we define the four-by-four matrix

$$\eta^{\alpha\beta} = \frac{1}{4}\tau_{ab}^\alpha\eta_{abcd}\tau_{cd}^\beta \tag{M.15}$$

in which there is a sum on repeated indices. With these definitions, Eq. (M.11) can be written as:

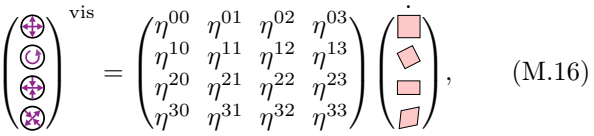

$$= \begin{pmatrix} \eta^{00} & \eta^{01} & \eta^{02} & \eta^{03} \\ \eta^{10} & \eta^{11} & \eta^{12} & \eta^{13} \\ \eta^{20} & \eta^{21} & \eta^{22} & \eta^{23} \\ \eta^{30} & \eta^{31} & \eta^{32} & \eta^{33} \end{pmatrix}$$

(M.16)

where the superscript "vis" denotes the viscous stresses. Certain physical assumptions restrict the form of $\eta^{\alpha\beta}$. For example, in an isotropic system (without any other constraint), $\eta^{\alpha\beta}$ takes the form [23]:

$$\eta^{\alpha\beta} = \begin{pmatrix} \zeta & \eta^{\mathrm{B}} & 0 & 0 \\ \eta^{\mathrm{A}} & \eta^{\mathrm{R}} & 0 & 0 \\ 0 & 0 & \eta & \eta^{\mathrm{o}} \\ 0 & 0 & -\eta^{\mathrm{o}} & \eta \end{pmatrix}. \tag{M.17}$$

The Cartesian tensors are reconstructed using

$$\sigma_{ab} = \sigma^{\alpha}\, \tau^{\alpha}_{ab} \quad \text{and} \quad \dot{e}_{ab} = \frac{1}{2}\, \dot{e}^{\alpha}\, \tau^{\alpha}_{ab} \tag{M.18}$$

as well as

$$\eta_{abcd} = \eta^{\alpha\beta}\, \tau^{\alpha}_{ab}\, \tau^{\beta}_{cd}. \tag{M.19}$$

Here, we attribute no meaning to the position (subscript or superscript) of the indices (so for instance $\eta_{\alpha\beta}$ and $\eta^{\alpha\beta}$ mean exactly the same thing).
In standard tensor notation, Eq. (M.17) reads

$$\begin{aligned} \eta_{abcd} = {} & \zeta\, \delta_{ab}\delta_{cd} - \eta^{\mathrm{A}}\epsilon_{ab}\delta_{cd} - \eta^{\mathrm{B}}\delta_{ab}\epsilon_{cd} + \eta^{\mathrm{R}}\epsilon_{ab}\epsilon_{cd} \\ & + \eta\, (\delta_{ac}\delta_{bd} + \delta_{ad}\delta_{bc} - \delta_{ab}\delta_{cd}) + \eta^{\mathrm{o}} E_{abcd} \end{aligned} \tag{M.20}$$

where δ_{ab} and ϵ_{cd} denote the Kronecker delta and Levi-Civita tensors (note that $\epsilon_{ab} = \tau^{1}_{ba}$), respectively, and

$$E_{abcd} = \frac{1}{2}(\epsilon_{ac}\delta_{bd} + \epsilon_{ad}\delta_{bc} + \epsilon_{bd}\delta_{ac} + \epsilon_{bc}\delta_{ad}). \tag{M.21}$$

(Equivalently, $E_{abcd} = \epsilon_{ac}\delta_{bd} + \epsilon_{bd}\delta_{ac}$.)

When the viscosity coefficients do not depend on space, the Navier-Stokes equation

$$\rho \mathrm{D}_t \mathbf{u} = \boldsymbol{\nabla} \cdot \boldsymbol{\sigma} \quad \text{i.e.} \quad \rho \mathrm{D}_t u_a = \partial_b \sigma_{ab} \tag{M.22}$$

takes in isotropic chiral active fluids the general form

$$\begin{aligned} \rho \mathrm{D}_t \mathbf{u} = {} & \boldsymbol{\nabla} \cdot \boldsymbol{\sigma}_{\mathrm{ss}} + \zeta\ \mathrm{grad}(\mathrm{div}\, \mathbf{u}) + \eta\, \Delta \mathbf{u} + \eta^{\mathrm{o}}\, \epsilon \cdot \Delta \mathbf{u} \\ & - \eta^{\mathrm{A}}\, \epsilon \cdot \mathrm{grad}(\mathrm{div}\, \mathbf{u}) + \eta^{\mathrm{B}}\ \mathrm{grad}(\mathrm{rot}\, \mathbf{u}) \\ & - \eta^{\mathrm{R}}\, \epsilon \cdot \mathrm{grad}(\mathrm{rot}\, \mathbf{u}) \end{aligned} \tag{M.23}$$

where $\mathrm{rot}\, \mathbf{u} = \epsilon_{ab}\partial_a u_b$ and

$$\epsilon = \begin{pmatrix} 0 & 1 \\ -1 & 0 \end{pmatrix} \tag{M.24}$$

is the rotation matrix by $-\pi/2$.

C. Derivation of the fluctuating hydrodynamic theory with the Mori-Zwanzig formalism

Here we derive the fluctuating hydrodynamic theory for chiral active fluids, by using the Mori-Zwanzig formalism [51, 84–86]. This formalism provides a systematic coarse-graining procedure to decompose the microscopic dynamics of a many-body system into hydrodynamic linear response and fluctuations induced by random stresses. Here, we give key steps of the derivation and refer the reader to Supplementary Sec. VI for more details.

We also direct the reader to Refs. [87, 88] and references therein for similar applications of the Mori-Zwanzig formalism in different contexts, and to Refs. [89, 90] for experimental investigations of the Green-Kubo relation for viscosities in dusty plasma and Ref. [91] for an analysis of the density-vorticity correlations in chiral active fluids with odd viscosities.

1. *Slow variables for momentum transfer*

The dynamics of a classical many-body system can be described by its state trajectory $\mathbf{\Gamma} = (\mathbf{p}^N, \mathbf{q}^N)$ in phase space, where N is the number of particles, $\mathbf{p}_i = m\mathbf{v}_i$ and $\mathbf{q}_i = \mathbf{r}_i$ are the momentum and position of a given particle i. For common fluids, this microscopic dynamics can be decomposed into a slow hydrodynamic behavior plus fast fluctuations around it. The slow hydrodynamic variables are typically conserved quantities (mass, momentum, etc.) and their conservation laws, such as the Navier–Stokes equations, describe the macroscopic dynamics of the system. Fluctuating hydrodynamics accounts for the fast fluctuations through the addition of a random stress in the Navier–Stokes equation for linear momentum [41, ch. IX]. These fluctuations are ignored in usual fluid mechanics, but can become important e.g. at the onset of hydrodynamic instabilities and in turbulent flows. Here we extend this treatment to the class of active fluids.

Similar to conventional hydrodynamic theory, we choose momentum density as the relevant slow variable to capture momentum transfer in active fluids. In particular, we define the wavevector-dependent (reciprocal space) momentum density of the system as

$$\hat{\mathbf{J}}_{\mathbf{k}}(t) \triangleq \sum_{i}^{N} m\mathbf{v}_i(t) \mathrm{e}^{-\mathrm{i}\mathbf{k}\cdot\mathbf{r}_i(t)}. \tag{M.25}$$

Taking the time derivative on the both sides, we obtain the governing equation of $\hat{\mathbf{J}}_{\mathbf{k}}(t)$:

$$\dot{\hat{\mathbf{J}}}_{\mathbf{k}}(t) = \mathrm{i}\mathbf{k} \cdot \hat{\boldsymbol{\sigma}}_{\mathbf{k}}(t), \tag{M.26}$$

where $\hat{\boldsymbol{\sigma}}_{\mathbf{k}}(t)$ is the wavevector-dependent stress

$$\hat{\boldsymbol{\sigma}}_{\mathbf{k}} \triangleq -\sum_{i}^{N} \left[m\mathbf{v}_i\mathbf{v}_i + \frac{1}{2} \sum_{j\neq i}^{N-1} \mathbf{f}_{ij}\mathbf{r}_{ij} \right] \mathrm{e}^{-\mathrm{i}\mathbf{k}\cdot\mathbf{r}_i}, \tag{M.27}$$

which consistently is also the Fourier transform of the Irving–Kirkwood formula Eq. (7).

Following the same procedure, we can also define the wavevector-dependent mass density

$$\rho_{\mathbf{k}}(t) \triangleq \sum_{i}^{N} m\mathrm{e}^{-\mathrm{i}\mathbf{k}\cdot\mathbf{r}_i(t)}, \tag{M.28}$$

and derive its governing equation:

$$\dot{\rho}_{\mathbf{k}}(t) = \mathrm{i}\mathbf{k}\cdot\hat{\mathbf{J}}_{\mathbf{k}}(t). \tag{M.29}$$

2. Steady-state ensemble

The active fluids considered here reach and sustain the steady state by balancing energy injection and dissipation at the microscopic level. As illustrated in Fig. 1 and Extended Figs. E1-E2, the passive degrees of freedom are in contact with an effective bath powered by the active degrees of freedom. This gives rise to a steady-state ensemble with a stationary distribution $f_0(\mathbf{\Gamma})$ in the phase space.

Any observable of the system (such as the momentum density $\hat{\mathbf{J}}_{\mathbf{k}}$) corresponds to a function defined on phase space. These phase-space functions form a Hilbert space, which we denote as $\mathscr{H}(\mathbf{\Gamma})$. Using the probability measure $f_0(\mathbf{\Gamma})$, we can define the following inner product on the space $\mathscr{H}(\mathbf{\Gamma})$:

$$(A,B) = \big\langle A(\mathbf{\Gamma})B^*(\mathbf{\Gamma})\big\rangle \triangleq \int \mathrm{d}\mathbf{\Gamma} A(\mathbf{\Gamma})B^*(\mathbf{\Gamma})f_0(\mathbf{\Gamma}) \tag{M.30}$$

where $A(\mathbf{\Gamma})$ and $B(\mathbf{\Gamma})$ are two arbitrary phase-space functions, * denotes complex conjugate, and the notation $\langle\ \rangle$ defined in Eq. (M.30) denotes the ensemble average over $f_0(\mathbf{\Gamma})$. This inner product measures the similarity between two observables under the steady-state ensemble, and will allow us to separate slow and fast variables on $\mathscr{H}(\mathbf{\Gamma})$ by defining an orthogonal projection. Given two vectors of phase-space functions $\mathbf{A}$ and $\mathbf{B}$ with components A_p and B_p, we also define the matrix $(\mathbf{A}\otimes\mathbf{B})$ with matrix elements

$$(\mathbf{A}\otimes\mathbf{B})_{pq} = (A_p, B_q). \tag{M.31}$$

This is an outer product of the vectors combined with an inner product of the phase-space functions.

Let us consider the slow variable $\hat{\mathbf{J}}_{\mathbf{k}}$, which is in fact a vector-valued function $\hat{\mathbf{J}}_{\mathbf{k}}(\mathbf{\Gamma}) = (\hat{J}_{\mathbf{k},1}(\mathbf{\Gamma}),\dots,\hat{J}_{\mathbf{k},D}(\mathbf{\Gamma}))^{\mathrm{T}}$, where D is the dimension of the system. Its different components generate a subspace $\mathscr{S}_{\hat{\mathbf{J}}_{\mathbf{k}}}(\mathbf{\Gamma})$, and the projection operator

$$\mathcal{P}_{\mathbf{k}}\mathbf{X}(\mathbf{\Gamma}) \triangleq (\mathbf{X}\otimes\hat{\mathbf{J}}_{\mathbf{k}})\cdot(\hat{\mathbf{J}}_{\mathbf{k}}\otimes\hat{\mathbf{J}}_{\mathbf{k}})^{-1}\cdot\hat{\mathbf{J}}_{\mathbf{k}} \tag{M.32}$$

performs an orthogonal projection on this subspace. We also define the projection operator to the orthogonal subspace:

$$\mathcal{Q}_{\mathbf{k}} = \mathbb{1} - \mathcal{P}_{\mathbf{k}}. \tag{M.33}$$

In Eq. (M.32), the normalization matrix $(\hat{\mathbf{J}}_{\mathbf{k}}\otimes\hat{\mathbf{J}}_{\mathbf{k}})$ quantifies the correlations between different components of the momentum density at the steady state, with form

$$(\hat{\mathbf{J}}_{\mathbf{k}}\otimes\hat{\mathbf{J}}_{\mathbf{k}}) = m^2N\left[\frac{k_{\mathrm{B}}T_{\mathrm{eff}}}{m}\mathcal{I} + n\hat{\mathcal{C}}_{\mathbf{vv}}(\mathbf{k})\right], \tag{M.34}$$

where $\mathcal{I}$ is a $D\times D$ identity matrix and n is the number density of the particles, $\hat{\mathcal{C}}_{\mathbf{vv}}(\mathbf{k})$ is the Fourier transform of the velocity–velocity correlation matrix

$$\hat{\mathcal{C}}_{\mathbf{vv}}(\mathbf{r}) = \big\langle\mathbf{v}(\mathbf{r})\,\mathbf{v}(0)\big\rangle. \tag{M.35}$$

In common fluids, interactions between fluid particles are conservative and only depend on interparticle distance. This allows the factorization of the Boltzmann distribution into momentum and position parts:

$$P(\mathbf{\Gamma}) \propto \mathrm{e}^{-\sum_i mv_i^2/2k_{\mathrm{B}}T}\times\mathrm{e}^{-\sum_{ij}U(\mathbf{r}_{ij})/k_{\mathrm{B}}T}. \tag{M.36}$$

Hence the velocities of different particles are independent, and $\hat{\mathcal{C}}_{\mathbf{vv}}(\mathbf{k})$ vanishes.

However, this is not generally the case for non-equilibrium fluid involved with velocity-dependent interactions, including our chiral active fluid. By assuming the isotropy of the system and a fast decaying correlation function $|\hat{\mathcal{C}}_{\mathbf{vv}}(\mathbf{r})| < \mathcal{O}(r^{-D})$, we show that

$$(\hat{\mathbf{J}}_{\mathbf{k}}\otimes\hat{\mathbf{J}}_{\mathbf{k}}) \approx Nm\,(k_{\mathrm{B}}T_{\mathrm{eff}} + B_{\mathbf{vv}})\,\mathcal{I}, \tag{M.37}$$

in which

$$B_{\mathbf{vv}} \triangleq \frac{nm}{D}\lim_{\mathbf{k}\to0}\int_V \big\langle\mathbf{v}(\mathbf{r})\cdot\mathbf{v}(0)\big\rangle\,\mathrm{e}^{-\mathrm{i}\mathbf{k}\cdot\mathbf{r}}\mathrm{d}\mathbf{r}. \tag{M.38}$$

For convenience, we define

$$T^*_{\mathrm{eff}} = T_{\mathrm{eff}} + B_{\mathbf{vv}}/k_{\mathrm{B}}. \tag{M.39}$$

3. Mori-Zwanzig formalism

Now we can use the projection operators $\mathcal{P}_{\mathbf{k}}$ and $\mathcal{Q}_{\mathbf{k}}$ to decompose the evolution of momentum density $\hat{\mathbf{J}}_{\mathbf{k}}$ into a slow dynamics within the subspace $\mathscr{S}_{\hat{\mathbf{J}}_{\mathbf{k}}}(\mathbf{\Gamma})$ and fast fluctuations orthogonal to it. This is the main idea of the Mori-Zwanzig formalism.

One can show that the governing equation Eq. (M.26) is also a Liouvillian equation:

$$\dot{\hat{\mathbf{J}}}_{\mathbf{k}}(t) = \mathrm{i}\mathcal{L}\hat{\mathbf{J}}_{\mathbf{k}}(t) \tag{M.40}$$

where

$$\mathrm{i}\mathcal{L} \triangleq \dot{\mathbf{\Gamma}}\cdot\frac{\partial}{\partial\mathbf{\Gamma}} \tag{M.41}$$

denotes the Liouville operator. Using the Mori-Zwanzig formalism, we decompose the above equation as

$$\dot{\hat{\mathbf{J}}}_{\mathbf{k}}(t) = \mathbf{F}^{\parallel}_{\mathbf{k}}(t) + \mathbf{F}^{\perp}_{\mathbf{k}}(t) - \int_0^t \mathbf{K}(\tau)\cdot\hat{\mathbf{J}}_{\mathbf{k}}(t-\tau)\,\mathrm{d}\tau \tag{M.42}$$

where

$$\mathbf{F}^{\parallel}_{\mathbf{k}}(t) \triangleq \mathrm{e}^{\mathrm{i}\mathcal{L}t}\mathcal{P}_{\mathbf{k}}\mathrm{i}\mathcal{L}\hat{\mathbf{J}}_{\mathbf{k}}(\mathbf{\Gamma}), \tag{M.43}$$

$$\mathbf{F}^{\perp}_{\mathbf{k}}(t) \triangleq \mathrm{e}^{\mathcal{Q}_{\mathbf{k}}\mathrm{i}\mathcal{L}t}\mathcal{Q}_{\mathbf{k}}\mathrm{i}\mathcal{L}\hat{\mathbf{J}}_{\mathbf{k}}(\mathbf{\Gamma}), \tag{M.44}$$

$$\mathbf{K}(\tau) \triangleq (\mathbf{F}^{\perp}_{\mathbf{k}}(\tau)\otimes\mathbf{F}^{\perp}_{\mathbf{k}}(0))\cdot(\hat{\mathbf{J}}_{\mathbf{k}}\otimes\hat{\mathbf{J}}_{\mathbf{k}})^{-1}. \tag{M.45}$$

Here, $\mathbf{F}^{\parallel}_{\mathbf{k}}(\mathbf{\Gamma},t)$ and $\mathbf{F}^{\perp}_{\mathbf{k}}(\mathbf{\Gamma},t)$ are the components of the generalized force $\mathrm{i}\mathcal{L}\hat{\mathbf{J}}_{\mathbf{k}}(t)$ parallel and orthogonal to the subspace $\mathscr{S}_{\hat{\mathbf{J}}_{\mathbf{k}}}(\mathbf{\Gamma})$, $\mathbf{K}(\tau)$ is a kernel function characterizing the linear response of the fluid towards external disturbances on $\hat{\mathbf{J}}_{\mathbf{k}}$. Note that $\mathbf{K}(\tau)$ involves the calculation of time correlation functions, which requires performing ensemble average at different time points. For systems with deterministic microscopic dynamics, we can generalize Eq. (M.30) to calculate time correlation function with equal-time probability $f_0(\mathbf{\Gamma})$:

$$\begin{aligned}&\big(A(t),B(0)\big)=\big\langle A(\mathbf{\Gamma}_t)B^*(\mathbf{\Gamma}_0)\big\rangle\\&=\int \mathrm{d}\mathbf{\Gamma}\ \mathcal{Q}_A(\mathbf{\Gamma},t)A(\mathbf{\Gamma})\cdot B(\mathbf{\Gamma})\cdot f_0(\mathbf{\Gamma}),\end{aligned} \tag{M.46}$$

where $\mathcal{Q}_A(\mathbf{\Gamma},t)$ is the propagator of the phase-space function A, and we have used $\mathbf{\Gamma}=\mathbf{\Gamma}_0$ to represent the phase space at the initial state $t=0$. In the case of Eq. (M.45), $A=B=\mathbf{F}^{\perp}_{\mathbf{k}}$, $\mathcal{Q}_A(\mathbf{\Gamma},t)=\mathrm{e}^{\mathcal{Q}_{\mathbf{k}}\mathrm{i}\mathcal{L}t}$.

Extra care must be taken when applying the formalism to active fluids. A crucial step in the derivation of Eq. (M.42):

$$(\mathrm{i}\mathcal{L}\mathbf{F}^{\perp}_{\mathbf{k}}(\tau)\otimes\hat{\mathbf{J}}_{\mathbf{k}}) = -(\mathbf{F}^{\perp}_{\mathbf{k}}(\tau)\otimes\mathrm{i}\mathcal{L}\hat{\mathbf{J}}_{\mathbf{k}}). \tag{M.47}$$

A key insight is that this relation still holds near any nonequilibrium steady state, even when detailed balance is broken. At the steady state, the probability distribution does not change over time, thus

$$\frac{\mathrm{d}}{\mathrm{d}t}f_0(\mathbf{\Gamma}) = \frac{\partial}{\partial\mathbf{\Gamma}}(\dot{\mathbf{\Gamma}}f_0(\mathbf{\Gamma})) = 0. \tag{M.48}$$

Given the assumption of the existence of a steady state, one can prove Eq. (M.47) elementwise using integration by parts:

$$\begin{aligned}&(\mathrm{i}\mathcal{L}\mathbf{F}^{\perp}_{\mathbf{k}}(\tau)\otimes\hat{\mathbf{J}}_{\mathbf{k}})_{ab}+(\mathbf{F}^{\perp}_{\mathbf{k}}(\tau)\otimes\mathrm{i}\mathcal{L}\hat{\mathbf{J}}_{\mathbf{k}})_{ab}\\&=-\int \mathrm{d}\mathbf{\Gamma}F^{\perp}_{\mathbf{k},a}(\mathbf{\Gamma},\tau)\hat{J}^{*}_{\mathbf{k},b}(\mathbf{\Gamma})\cdot\frac{\partial}{\partial\mathbf{\Gamma}}(\dot{\mathbf{\Gamma}}f_0(\mathbf{\Gamma}))=0.\end{aligned} \tag{M.49}$$

In this case, the Liouvillian is Hermitian with respect to the inner product defined by f_0 and the decomposition given by Eq. (M.42) still holds.

4. Generalized forces

To make use of the Mori-Zwanzig formalism, we must derive the explicit form of $\mathbf{F}^{\parallel}_{\mathbf{k}}$, $\mathbf{F}^{\perp}_{\mathbf{k}}$ and $\mathbf{K}$.

For active fluids, the generalized force contains three components:

$$\mathrm{i}\mathcal{L}\hat{\mathbf{J}}_{\mathbf{k}} = \mathrm{i}\mathbf{k}\cdot\hat{\boldsymbol{\sigma}}_{\mathbf{k}} = \mathrm{i}\mathbf{k}\cdot\left(\hat{\boldsymbol{\sigma}}^{\mathrm{kin}}_{\mathbf{k}}+\hat{\boldsymbol{\sigma}}^{\mathrm{pos}}_{\mathbf{k}}+\hat{\boldsymbol{\sigma}}^{\mathrm{vel}}_{\mathbf{k}}\right), \tag{M.50}$$

with

$$\hat{\boldsymbol{\sigma}}^{\mathrm{kin}}_{\mathbf{k}} \triangleq -\sum_{i}^{N} m\mathbf{v}_i\mathbf{v}_i\,\mathrm{e}^{-\mathrm{i}\mathbf{k}\cdot\mathbf{r}_i} \tag{M.51}$$

$$\hat{\boldsymbol{\sigma}}^{\mathrm{pos}}_{\mathbf{k}} \triangleq -\frac{1}{2}\sum_{ij}^{N^2}\mathbf{f}^{\mathrm{pos}}_{ij}\,\mathbf{r}_{ij}\mathrm{e}^{-\mathrm{i}\mathbf{k}\cdot\mathbf{r}_i}, \tag{M.52}$$

$$\hat{\boldsymbol{\sigma}}^{\mathrm{vel}}_{\mathbf{k}} \triangleq -\frac{1}{2}\sum_{ij}^{N^2}\mathbf{f}^{\mathrm{vel}}_{ij}\,\mathbf{r}_{ij}\mathrm{e}^{-\mathrm{i}\mathbf{k}\cdot\mathbf{r}_i}, \tag{M.53}$$

where $\hat{\boldsymbol{\sigma}}^{\mathrm{kin}}_{\mathbf{k}}$ is the kinetic stress, $\hat{\boldsymbol{\sigma}}^{\mathrm{pos}}_{\mathbf{k}}$ is the virial stress only involving the position-dependent interactions $\mathbf{f}^{\mathrm{pos}}_{ij}$, and $\hat{\boldsymbol{\sigma}}^{\mathrm{vel}}_{\mathbf{k}}$ is the virial stress caused by velocity-dependent interactions, which is unique to nonequilibrium fluids. Here we assume the velocity-dependent interactions come from interparticle friction, taking a general form $\mathbf{f}^{\mathrm{vel}}_{ij} = -\gamma(r_{ij})\,\mathbf{v}_{ij}$.

The presence of the interparticle friction as well as the resultant velocity–velocity correlations poses a major challenge in our derivation, making it different from the textbook derivation of the Green–Kubo relation for viscosity using the Mori-Zwanzig formalism [86]. By assuming that the three-body (and higher order) correlations are negligible, we can derive the explicit form of the generalized forces:

$$\mathbf{F}^{\parallel}_{\mathbf{k}}(t) = -\gamma_{\hat{\mathbf{J}}_{\mathbf{k}}}\hat{\mathbf{J}}_{\mathbf{k}}(t), \tag{M.54}$$

$$\mathbf{F}^{\perp}_{\mathbf{k}}(t) \approx \gamma_{\hat{\mathbf{J}}_{\mathbf{k}}}\hat{\mathbf{J}}_{\mathbf{k}}(t) + \mathrm{i}\mathbf{k}\cdot\hat{\boldsymbol{\sigma}}_{\mathbf{k}}(t), \tag{M.55}$$

where $\gamma_{\hat{\mathbf{J}}_{\mathbf{k}}} = n(\hat{\gamma}(0)-\hat{\gamma}(k))/m$ denotes the wavevector-dependent effective damping parameter for $\hat{\mathbf{J}}_{\mathbf{k}}$. Here $\hat{\gamma}(k)=\int_V\gamma(r)\mathrm{e}^{-\mathrm{i}\mathbf{k}\cdot\mathbf{r}}\mathrm{d}\mathbf{r}$ denotes the Fourier transform of the interparticle frictional kernel $\gamma(r)$. With that, we can also derive the form of the response kernel:

$$\begin{aligned}\mathbf{K}(\tau) = &-\gamma^2_{\hat{\mathbf{J}}_{\mathbf{k}}}\big(\hat{\mathbf{J}}_{\mathbf{k}}(\tau)\otimes\hat{\mathbf{J}}_{\mathbf{k}}(0)\big)\cdot(\hat{\mathbf{J}}_{\mathbf{k}}\otimes\hat{\mathbf{J}}_{\mathbf{k}})^{-1}\\&+\big(\mathrm{i}\mathbf{k}\cdot\hat{\boldsymbol{\sigma}}_{\mathbf{k}}(\tau)\otimes\mathrm{i}\mathbf{k}\cdot\hat{\boldsymbol{\sigma}}_{\mathbf{k}}(0)\big)\cdot(\hat{\mathbf{J}}_{\mathbf{k}}\otimes\hat{\mathbf{J}}_{\mathbf{k}})^{-1}.\end{aligned} \tag{M.56}$$

Detailed derivation steps are provided in the Supplementary Sec. VI.

5. Green–Kubo relation

For a system in a nonequilibrium steady state, the noise term $\mathbf{F}^{\perp}_{\mathbf{k}}$ vanishes in Eq. (M.42) under an ensemble average. Thus in an average sense, the governing equation Eq. (M.26) reads

$$\dot{\hat{\mathbf{J}}}_{\mathbf{k}}(t) = \mathbf{F}^{\parallel}_{\mathbf{k}}(t) - \int_0^t \mathrm{d}\tau\ \mathbf{K}(\tau)\cdot\hat{\mathbf{J}}_{\mathbf{k}}(t-\tau). \tag{M.57}$$

By plugging the explicit form of $\mathbf{F}^{\parallel}_{\mathbf{k}}$ and $\mathbf{K}$ and taking Laplace transform, we can obtain the following equation:

$$s\tilde{\mathbf{J}}_{\mathbf{k}}(s) - \hat{\mathbf{J}}_{\mathbf{k}}(0) = -\frac{\big(\mathrm{i}\mathbf{k}\cdot\tilde{\boldsymbol{\sigma}}_{\mathbf{k}}(s)\otimes\mathrm{i}\mathbf{k}\cdot\hat{\boldsymbol{\sigma}}_{\mathbf{k}}(0)\big)\cdot\tilde{\mathbf{J}}_{\mathbf{k}}(s)}{Nmk_{\mathrm{B}}T^{*}_{\mathrm{eff}}}. \tag{M.58}$$

Note that the right-hand side of the above equation is a linear response in momentum density $\hat{\mathbf{J}}_{\mathbf{k}}$. Given the wavevector-dependent strain rate $\hat{\dot{e}}_{\mathbf{k},cd} = \mathrm{i}k_d\hat{J}_{\mathbf{k},c}/nm$, we find that Eq. (M.58) in fact corresponds to a hydrodynamic linear response

$$s\tilde{J}_{\mathbf{k},a}(s) - \hat{J}_{\mathbf{k},a}(0) = \mathrm{i}k_b\,\tilde{\eta}_{\mathbf{k},abcd}(s)\,\tilde{\dot{e}}_{\mathbf{k},cd}(s) \tag{M.59}$$

with viscosity coefficients

$$\tilde{\eta}_{\mathbf{k},abcd}(s) \triangleq \frac{1}{k_{\mathrm{B}}T^{*}_{\mathrm{eff}}V}\big\langle\tilde{\sigma}_{\mathbf{k},ab}(s)\hat{\sigma}^{*}_{\mathbf{k},cd}(0)\big\rangle. \tag{M.60}$$

Here we switched to index notation and used the Einstein summation rule for the indices. In the hydrodynamic limit, Eq. (M.60) becomes the equilibrium-like Green–Kubo relation for the viscosity

$$\eta_{abcd} = \lim_{\substack{\mathbf{k}\to\mathbf{0}\\ s\to 0}}\tilde{\eta}_{\mathbf{k},abcd}(s) = \frac{V}{k_{\mathrm{B}}T^{*}_{\mathrm{eff}}}\int_0^\infty\big\langle\sigma_{ab}(t)\sigma_{cd}(0)\big\rangle\mathrm{d}t, \tag{M.61}$$

which is equivalent to Eq. (11) in terms of the irreducible representations of stress. Note that in the above formula, we have used the global stress $\boldsymbol{\sigma}(t) = \int_V\boldsymbol{\sigma}(\mathbf{r},t)\,\mathrm{d}\mathbf{r}\,/\,V$.

6. *Hydrodynamic equations*

Our previous derivation was performed near a steady state with a vanishing background flow field $\mathbf{u}(\mathbf{r}) = 0$ everywhere. Here we extend our theory to the hydrodynamic behavior with nonzero background flow field. Let us first define the density, momentum and stress fields:

$$\rho(\mathbf{r}) = \sum_i^N m\,\delta(\mathbf{r}-\mathbf{r}_i), \tag{M.62}$$

$$\mathbf{J}(\mathbf{r}) = \sum_i^N m\mathbf{v}_i\,\delta(\mathbf{r}-\mathbf{r}_i), \tag{M.63}$$

$$\boldsymbol{\sigma}(\mathbf{r}) = -\sum_i^N\left[m\mathbf{v}_i\mathbf{v}_i + \frac{1}{2}\sum_{j\neq i}^{N-1}\mathbf{f}_{ij}\mathbf{r}_{ij}\right]\delta(\mathbf{r}-\mathbf{r}_i). \tag{M.64}$$

Note that they are also the inverse Fourier transforms of $\rho_{\mathbf{k}}$, $\hat{\mathbf{J}}_{\mathbf{k}}$ and $\hat{\boldsymbol{\sigma}}_{\mathbf{k}}$ defined previously. In addition, the flow field is defined as

$$\mathbf{u}(\mathbf{r}) = \frac{\mathbf{J}(\mathbf{r})}{\rho(\mathbf{r})}, \tag{M.65}$$

In a common fluid, the fluid elements stay near local thermal equilibrium. Similarly, we assume that the particles in an active fluid stay close to local steady state. Under these assumptions, we can decompose the particle velocity as

$$\mathbf{v} = \mathbf{u}(\mathbf{r},t) + \Delta\mathbf{v}, \tag{M.66}$$

where $\mathbf{u}(\mathbf{r},t)$ is the local flow field and $\Delta\mathbf{v}$ is the velocity fluctuation on top of it. These two terms satisfy

$$\big\langle\Delta\mathbf{v}\big\rangle = 0, \qquad \big\langle\mathbf{u}(\mathbf{r},t)\,\Delta\mathbf{v}\big\rangle = 0. \tag{M.67}$$

The interaction of a particle with its neighbors depends on their relative velocity, rather than their average velocity. Thus, we assume that, by subtracting the local flow field $\mathbf{u}(\mathbf{r})$, the local ensemble is the same as the global one at the steady state. This allows us to decompose the stress field $\boldsymbol{\sigma}(\mathbf{r})$ as

$$\boldsymbol{\sigma} = -\rho\mathbf{u}\mathbf{u} + \boldsymbol{\sigma}^{\mathrm{IK}} \tag{M.68}$$

where $\rho\mathbf{u}\mathbf{u}$ is the dynamical pressure due to fluid flow and $\boldsymbol{\sigma}^{\mathrm{IK}}$ is the Irving–Kirkwood stress,

$$\boldsymbol{\sigma}^{\mathrm{IK}}(\mathbf{r}) \triangleq -\sum_i^N\left[m\Delta\mathbf{v}_i\Delta\mathbf{v}_i + \frac{1}{2}\sum_{j\neq i}^{N-1}\mathbf{f}_{ij}\mathbf{r}_{ij}\right]\delta(\mathbf{r}-\mathbf{r}_i). \tag{M.69}$$

The Irving–Kirkwood stress can be further decomposed into three parts: (i) the isotropic steady-state stress given by the equations of state

$$\sigma^{\mathrm{ss}}_{ab} = \begin{cases} -P\,\delta_{ab} + \tau\,\epsilon_{ab}, & \text{in 2D}\\ -P\,\delta_{ab}, & \text{in 3D}\end{cases} \tag{M.70}$$

[in 3D, the presence of an antisymmetric steady-state stress is prohibited by isotropy] (ii) the viscous stress due to hydrodynamic linear response

$$\sigma^{\mathrm{vis}}_{ab} = \eta_{abcd}\,\dot{e}_{cd}, \tag{M.71}$$

and (iii) the random stress arising from the orthogonal generalized force satisfying the relation

$$\mathrm{i}k_b\,\hat{\sigma}^{\mathrm{R}}_{\mathbf{k},ab} = \hat{F}^{\perp}_{\mathbf{k},a} \tag{M.72}$$

With that, we can then get the hydrodynamic equations by performing the inverse Fourier transform of Eq. (M.26) and Eq. (M.29), giving

$$D_t\rho = -\rho\boldsymbol{\nabla}\cdot\mathbf{u}, \tag{M.73a}$$

$$\rho D_t\mathbf{u} = \boldsymbol{\nabla}\cdot\left(\boldsymbol{\sigma}^{\mathrm{ss}} + \boldsymbol{\sigma}^{\mathrm{vis}} + \boldsymbol{\sigma}^{\mathrm{R}}\right), \tag{M.73b}$$

where $D_t = \partial_t + \mathbf{u}\cdot\nabla$ is the material derivative.

7. *Random stress*

To complete our fluctuating hydrodynamic theory, we need to derive the form of the random stress $\boldsymbol{\sigma}^{\mathrm{R}}$. Recall

that the explicit form of the orthogonal generalized force is

$$\mathbf{F}^{\perp}_{\mathbf{k}}(t) \approx \gamma_{\hat{\mathbf{J}}_{\mathbf{k}}} \hat{\mathbf{J}}_{\mathbf{k}}(t) + \mathrm{i}\mathbf{k}\cdot\hat{\boldsymbol{\sigma}}_{\mathbf{k}}(t). \tag{M.74}$$

Using the homogeneity of the system at the steady state, we show that $\mathbf{F}^{\perp}_{\mathbf{k}}$ is indeed a random force with zero mean

$$\left\langle \mathbf{F}^{\perp}_{\mathbf{k}} \right\rangle = 0. \tag{M.75}$$

We also find that

$$\begin{aligned} \gamma_{\hat{\mathbf{J}}_{\mathbf{k}}} &= \frac{n}{m}\int_V \gamma(r)(1-\mathrm{e}^{-\mathrm{i}\mathbf{k}\cdot\mathbf{r}})\mathrm{d}\mathbf{r} \\ &= \left[\frac{2\pi n}{3m}\int_0^{\infty}\gamma(r) r^4 dr\right] k^2 + \mathcal{O}(k^3). \end{aligned} \tag{M.76}$$

Therefore, we can drop the first term in the calculation of the two-point correlations and get

$$\left\langle F^{\perp}_{\mathbf{k},a}(t)\, F^{\perp *}_{\mathbf{k},c}(0)\right\rangle \approx k_b \left\langle \hat{\sigma}_{\mathbf{k},ab}(t)\, \hat{\sigma}^{*}_{\mathbf{k},cd}(0)\right\rangle k_d. \tag{M.77}$$

Given the relation Eq. (M.60), one can further show

$$\left\langle \tilde{F}^{\perp}_{\mathbf{k},a}(s)\, F^{\perp *}_{\mathbf{k},c}(0)\right\rangle = k_{\mathrm{B}} T^{*}_{\mathrm{eff}} V\, \tilde{\eta}_{\mathbf{k},abcd}(s)\, k_b k_d. \tag{M.78}$$

Note that s is the parameter for Laplace transforms. Hence, we should construct the random stress $\boldsymbol{\sigma}^{\mathrm{R}}$ as

$$\left\langle \hat{\sigma}^{\mathrm{R}}_{\mathbf{k},ab}\right\rangle = 0, \tag{M.79}$$

$$\left\langle \hat{\sigma}^{\mathrm{R}}_{\mathbf{k},ab}(s)\, \hat{\sigma}^{\mathrm{R}*}_{\mathbf{k},cd}(0)\right\rangle = k_{\mathrm{B}} T^{*}_{\mathrm{eff}}\, \tilde{\eta}_{\mathbf{k},abcd}(s). \tag{M.80}$$

In the hydrodynamic limit, the correlation time and length of the random stress becomes negligible compared with that of the hydrodynamic flow. In this case, the above requirements can also be written as

$$\left\langle \sigma^{\mathrm{R}}_{ab}(\mathbf{r},t)\right\rangle = 0 \tag{M.81}$$

$$\left\langle \sigma^{\mathrm{R}}_{ab}(\mathbf{r},t)\sigma^{\mathrm{R}}_{cd}(0,0)\right\rangle = 2k_{\mathrm{B}}T^{*}_{\mathrm{eff}}\,\delta(\mathbf{r})\Big[\eta^{\mathrm{sym}}_{abcd}\delta(t) + \eta^{\mathrm{anti}}_{abcd}\xi(t)\Big]$$

where $\eta^{\mathrm{sym}}_{abcd} = (\eta_{abcd}+\eta_{cdab})/2$ and $\eta^{\mathrm{anti}}_{abcd} = (\eta_{abcd} - \eta_{cdab})/2$ are the symmetric and anti-symmetric parts of the viscosity tensor under the exchange of major indices, i.e. $ab \leftrightarrow cd$. In practice, the Dirac distribution in Eq. (M.81) has a finite width τ and can be represented, for instance, by a Gaussian function

$$\delta_\tau(t) \triangleq \frac{1}{\sqrt{2\pi}\,\tau}\mathrm{e}^{-\frac{t^2}{2\tau^2}}. \tag{M.82}$$

Similarly, $\xi(t)$ stands in Eq. (M.81) for a function $\xi_\tau(t)$ defined as

$$\xi_\tau(t) \triangleq \frac{t}{2\tau^2}\,\mathrm{e}^{-\frac{t^2}{2\tau^2}} \tag{M.83}$$

It is an odd function, satisfying the relations

$$\xi(t) = -\xi(-t), \qquad 2\int_0^{\infty}\xi(t)\,\mathrm{d}t = 1.$$

Upon decomposition of the stresses into their irreducible representations, Eq. (M.81) becomes Eq. (9) in the main text. By integrating Eq. (M.81) in both space and time, we get the Green–Kubo relation:

$$\int_0^{\infty}\mathrm{d}t\int_V \mathrm{d}\mathbf{r}\,\left\langle \sigma^{\mathrm{R}}_{ab}(\mathbf{r},t)\sigma^{\mathrm{R}}_{cd}(0,0)\right\rangle = k_{\mathrm{B}}T^{*}_{\mathrm{eff}}\eta_{abcd}. \tag{M.84}$$

We emphasize that the term $\eta^{\mathrm{anti}}_{abcd}\xi(t)$ changes sign when $t\to -t$. This is crucial to obtain the antisymmetric part of the viscosity tensor in the Green-Kubo relation, and consistent with intuitions from the usual Onsager-Casimir relations. For common fluids, the random stress is often chosen as a white noise in the conventional fluctuating hydrodynamic theory. However, for nonequilibrium fluids, especially chiral active fluids, extra care must be taken: the construction of the random stress should reflect the time-reversal symmetry/antisymmetry of the system.

Data availability

The data that supports all the plots in this paper is available at http://doi.org/10.5281/zenodo.5138328.

Code availability

The simulation codes used in this study are available upon request.

Acknowledgments

We thank A. G. Abanov, S. Atis, D. Bartolo, W. T. M. Irvine, C. Nardini, H. C. Öttinger, and D. T. Son for helpful discussions and suggestions. S.V., J.J.dP. and V.V. acknowledge primary support through the Chicago MRSEC, funded by the NSF through grant No. DMR-1420709. S.V. acknowledges support from the National Science Foundation under Grant No. DMR-1848306. V.V. acknowledges support from the Complex Dynamics and Systems Program of the Army Research Office under grant No. W911NF-19-1-0268, the Simons foundation, and the KITP program on Symmetry, Thermodynamics and Topology in Active Matter via NSF Grant No. PHY-1748958. M.H. and M.F. acknowledge support from the University of Chicago MRSEC through Kadanoff-Rice postdoctoral fellowships. C.S. acknowledges support by the National Science Foundation Graduate Research Fellowship under grant No. 1746045. M.H. acknowledges use of the GM4 cluster supported by the National Science Foundation's Division of Materials Research under the Major Research Instrumentation (MRI) program award No. 1828629. This work was completed in part with resources provided by the University of Chicago's Research Computing Center. Calculations presented here were performed on the GPU cluster supported by the NSF under Grant DMR-1828629.

Author contributions

M.H. performed the simulations and analyzed the data. All authors conducted theoretical research. M.H., M.F., C.S., and V.V. wrote the paper. All authors contributed to discussions, interpretation of the results, and manuscript revision.

Competing interests

The authors declare no competing financial interests.

EXTENDED DATA

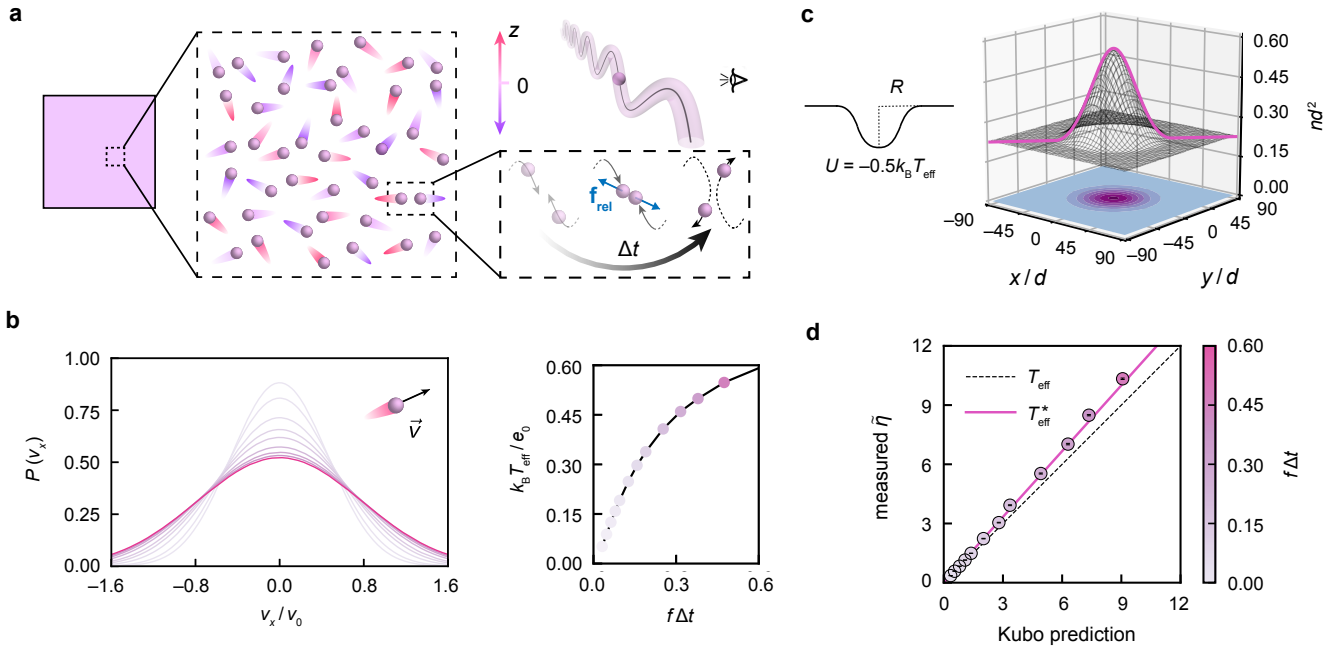

FIG. E1. **Thermodynamics of an oscillating granular gas. a.** Schematic of the system setup. We simulate a quasi-2D granular gas composed of frictional particles, which are forced to oscillate vertically at a constant frequency f but free to move horizontally. Interparticle collision between two oscillating particles could lead to their translational motions in the xy-plane. In the middle is a zoomed-in, top view of this many-body system. Horizontal translation of a particle is denoted by its tail, whereas its vertical oscillation is color-coded in the tail: gradient from a dark end to a bright front means the particle is moving towards the xy-plane, vice versa; purple denotes $z < 0$ whereas red denotes $z > 0$. Δt denotes the averaged collision duration. **b.** Maxwell distribution. The x-component of translational velocity displays a Gaussian distribution $P(v_x)$ at various oscillating frequency f. An effective temperature $T_{\rm eff}$ is defined using the halfwidth of $P(v_x)$. Dependence of $T_{\rm eff}$ on f is shown on the right. **c.** Boltzmann distribution. We put the system in a potential well $U(\mathbf{r}) = -0.5k_{\rm B}T_{\rm eff}\,[1+\cos(\pi r/R)]$ for $r < R$, where r denotes the distance from the center of the system. The resultant spatial distribution of the particles turns out to follow the Boltzmann statistics $n(-r) \propto \exp[-U(r)/k_{\rm B}T_{\rm eff}]$ (purple curve) as well. **d.** Green–Kubo relation. Shear viscosity of this many-body system can be either directly measured using linear response towards an applied shear or indirectly inferred from the Green–Kubo relation by calculating the integral of the stress–stress correlation function, known as the Green–Kubo relation. The predicted and measured shear viscosity η is compared at a wide range of frequencies f. The Kubo predictions with $T_{\rm eff}$ and renormalized $T^*_{\rm eff}$ are marked as the dashed and solid lines, respectively. We have defined $f_0 = 1/\Delta t$. Error bars denote standard errors.

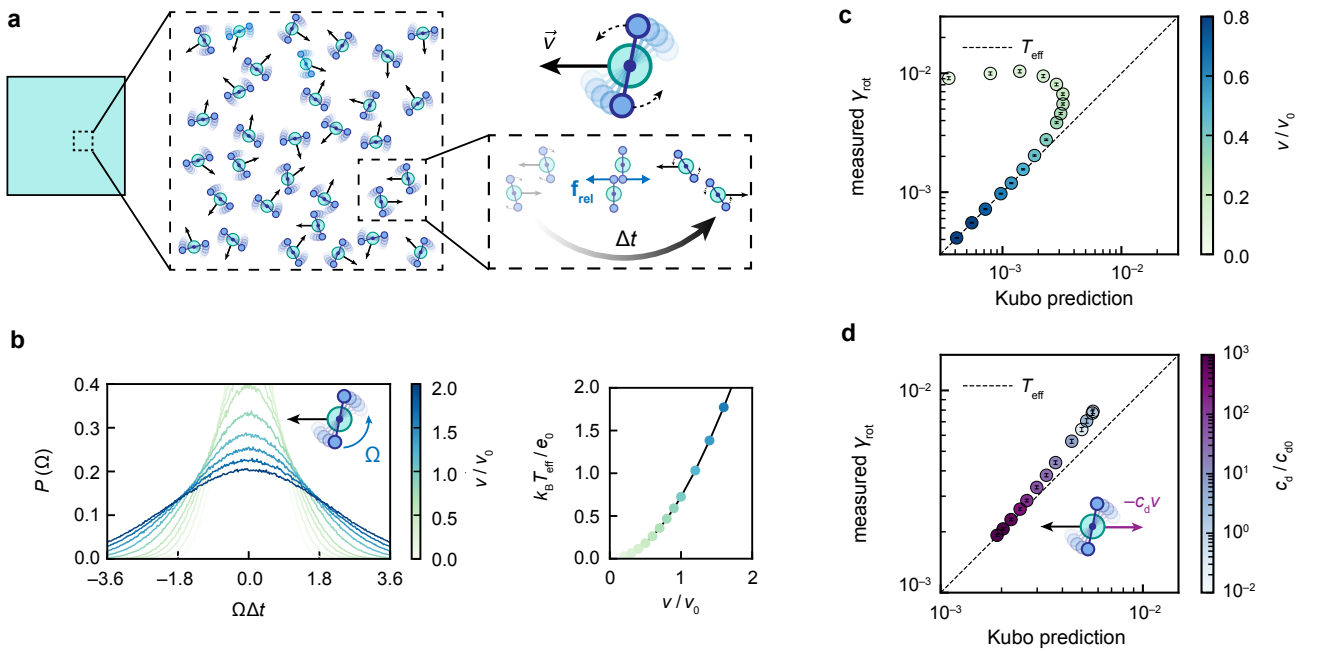

FIG. E2. **Thermodynamics of an active Brownian system. a.** Schematic of the system setup. We simulate a 2D system composed of active Brownian rollers. Each particle contains a core (in green) that self-propels nearly at a constant speed v meanwhile undergoes rotational diffusion as well as a dumbbell (in blue) that is hinged at the core center and free to rotate about it. In particular, the core of particle i is powered by an active force $\mathbf{F}_i^{\rm a} = c_{\rm d} v \hat{\mathbf{n}}_i$ ($\hat{\mathbf{n}}_i$ is the orientation of the core) meanwhile experiences a drag force by the substrate $\mathbf{F}_i^{\rm d} = -c_{\rm d}\mathbf{v}_i$, where ζ denotes the substrate friction coefficient. Note that the particle dumbbell is lifted away from the substrate thus does not experience any friction; moreover, the dumbbell rotation does not reorient the self-propulsion of the core. When two particles collide, the translational motion of the cores could result in the rotational motion of the dumbbells. Δt denotes the averaged collision duration. **b.** Maxwell distribution. The angular velocity of the dumbbells displays a Gaussian distribution $P(\Omega)$ at various self-propulsion speed v. An effective temperature $T_{\rm eff}$ is defined using the halfwidth of $P(\Omega)$. Dependence of $T_{\rm eff}$ on Ω is shown on the right. **c-d.** Green-Kubo relation. The rotational drag coefficient of the dumbbell can be either measured through linear response by measuring the terminal angular velocity under an applied torque, or predicted using the Green–Kubo relation by evaluating the integral of the torque–torque correlation function. The measured and predicted drag coefficient $\gamma_{\rm rot}$ is compared at a wide range of self-propulsion speed v (**c**) as well as substrate friction coefficient $c_{\rm d}$ (**d**). However, when either self-propulsion speed v or substrate friction coefficient $c_{\rm d}$ is increased, the relative significance of particle interaction compared to self-propulsion gets reduced. As a consequence, we see that the Green–Kubo relation is restored at either large v or $c_{\rm d}$. We have defined $v_0 = d/\Delta t$ and $c_{\rm d} = m/\Delta t$. Error bars denote standard errors.

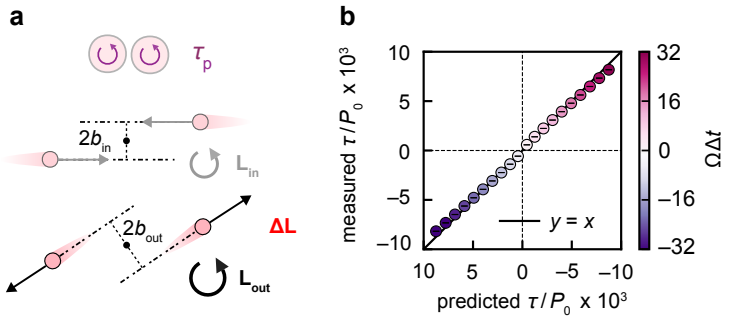

FIG. E3. **Microscopic origin of antisymmetric stress. a.** Schematic of orbital angular momentum change during collision. When two frictional active spinners collide, the angular momentum of self-spinning can be interchanged with the angular momentum of orbital motion around their center-of-mass, $L = mv_{\rm rel}b$, where $v_{\rm rel}$ is the relative moving speed of the particles and b is the impact parameter. The resultant change in the orbital angular momentum $\Delta L = L_{\rm out} - L_{\rm in}$ gives rise to effective antisymmetric stress exerted onto the chiral active fluid at the macroscopic level. In the Supplementary Sec. III, we provide a simple kinetic theory to derive the linear relation between antisymmetric stress τ and the average orbital angular momentum change $\overline{\Delta L}$ during collision, $\tau = \sqrt{\pi k_{\rm B} T_{\rm eff}/m}\cdot dn^2\cdot\overline{\Delta L}$. **b.** Validation of our kinetic theory. We measure the average orbital angular momentum change $\overline{\Delta L}$ by performing scattering simulations and then use it to predict the antisymmetric stress τ based upon the kinetic theory. The prediction on τ from $\overline{\Delta L}$ agrees well with the simulation measurement of a many-body system at the steady state. Error bars denote standard errors.

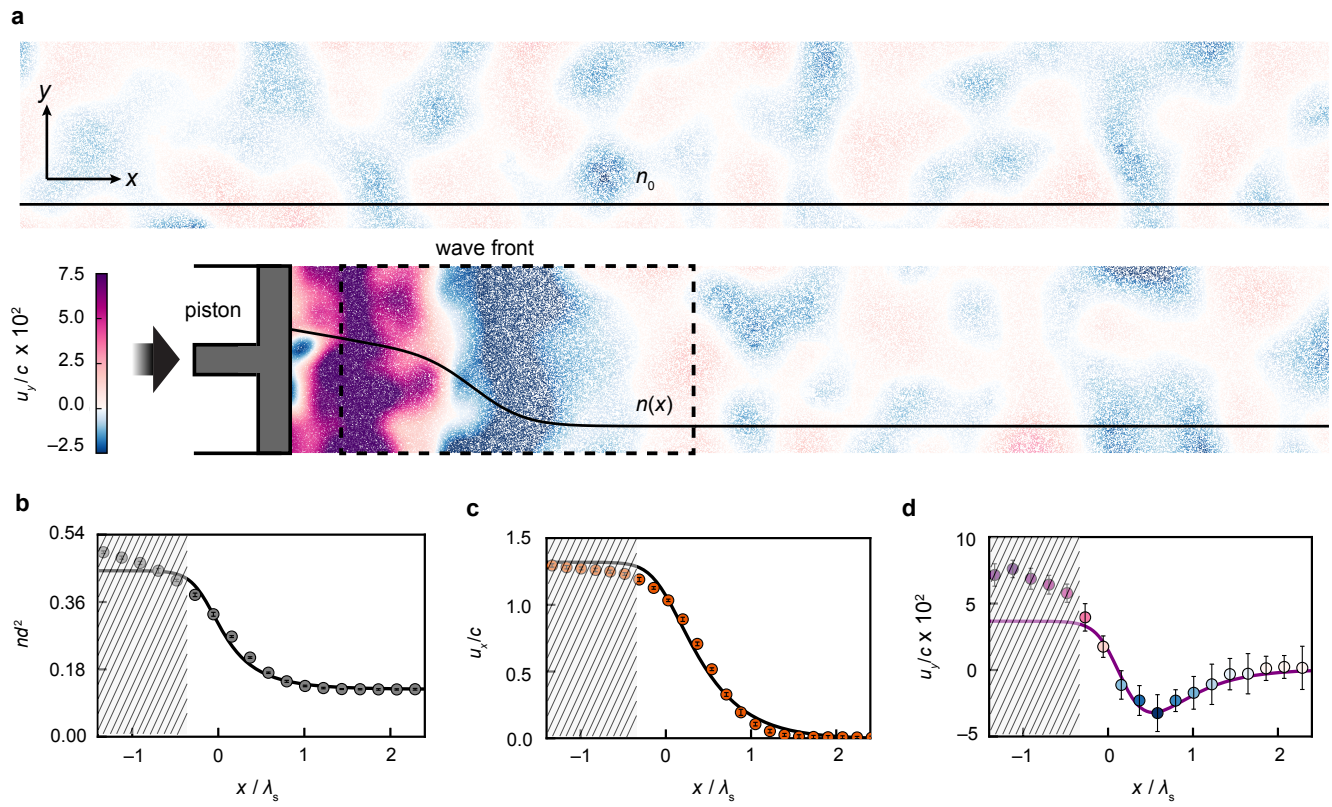

FIG. E4. **Transverse mode in a shock wave. a.** Shock wave. A piston moving at speed $U = 1.9d/\Delta t$ (faster than the speed of sound $c = 1.4d/\Delta t$) generates a shock wave accompanied with transverse flows, which is characterized by the vertical flow velocity u_y (gradient coloring). The particles self-spin counter-clockwise at speed $\Omega = 25.3/\Delta t$ and have an initial global density $n_0 = 0.125d^{-2}$. According to the viscid Burgers' equation $\partial_t u + u\partial_x u = \nu\partial_x^2 u$, the width of this shock is approximately $\lambda_s = 4\nu/U$, where $\nu = \eta/n_0 m$ is the kinematic viscosity. Hydrodynamic profiles are quantified near the wave front. Also see Supplementary Mov. S8. **b.** Density profile $n(x)$. The simulation results are compared with continuum hydrodynamic theory (solid line), which employs parameters measured in a separate homogeneous microscopic systems of number density n_0 (dashed line). Thus, theoretical predictions would break down at extreme densities (shaded region). **c.** Horizontal flow velocity $u_x(x)$. **d.** Vertical flow velocity $u_y(x)$. The same color coding as panel A is applied here. Predictions using continuum hydrodynamic theory are plotted as solid lines. Error bars denote standard errors.

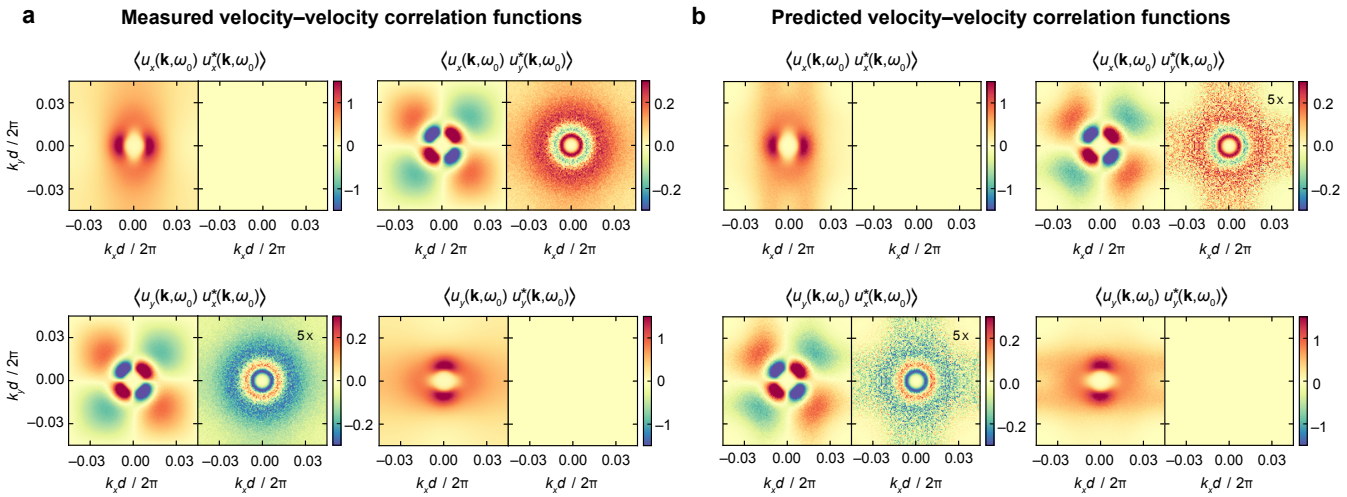

FIG. E5. **Power spectra of the velocity–velocity correlation functions** $\langle u_a(\mathbf{k},\omega)u_b^*(\mathbf{k},\omega)\rangle$**.** Here we compare the measured velocity–velocity correlation functions with the empirical prediction using fluctuating hydrodynamic theory. **a.** Correlation functions directly measured in the particle-based simulations of our chiral active fluid. **b.** Correlation functions predicted using the fluctuating hydrodynamic theory with the measured stress–stress correlation functions and viscosity tensor. The empirical prediction matches with the simulation results expect at very high k-modes, where the linear response approximation is no longer valid. Although the comparison is made at a given wave frequency $\omega_0 = 0.055\pi/\Delta t$, the consistency between direct measurements in simulations and predictions using fluctuating hydrodynamic theory generally holds at all wave frequencies.

[53] K. Drescher, K. C. Leptos, I. Tuval, T. Ishikawa, T. J. Pedley, and R. E. Goldstein, "Dancing volvox: hydrodynamic bound states of swimming algae," Phys. Rev. Lett. **102**, 168101 (2009).

[54] G. Kokot and A. Snezhko, "Manipulation of emergent vortices in swarms of magnetic rollers," Nat. Commun. **9**, 2344 (2018).

[55] Q.-L. Lei, M. P. Ciamarra, and R. Ni, "Nonequilibrium strongly hyperuniform fluids of circle active particles with large local density fluctuations," Sci. Adv. **5**, eaau7423 (2019).

[56] Q.-L. Lei and R. Ni, "Hydrodynamics of random-organizing hyperuniform fluids," Proc. Natl. Acad. Sci. U.S.A. **116**, 22983–22989 (2019).

[57] S. Plimpton, A. Kohlmeyer, A. Thompson, S. Moore, and R. Berger, "Lammps stable release 29 october 2020," (2020).

[58] S. Plimpton, "Fast parallel algorithms for short-range molecular dynamics," J. Comput. Phys. **117**, 1–19 (1995).

[59] M. Han, J. Yan, S. Granick, and E. Luijten, "Effective temperature concept evaluated in an active colloid mixture," Proc. Natl. Acad. Sci. U.S.A. **114**, 7513–7518 (2017).

[60] J. Yan, S. C. Bae, and S. Granick, "Rotating crystals of magnetic janus colloids," Soft Matter **11**, 147–153 (2015).

[61] C. J. Reeves, I. S. Aranson, and P. M. Vlahovska, "Emergence of lanes and turbulent-like motion in active spinner fluid," Commun. Phys. **4** (2021), 10.1038/s42005-021-00596-2.

[62] L. Le Goff, F. Amblard, and E. M. Furst, "Motor-driven dynamics in actin-myosin networks," Phys. Rev. Lett. **88**, 018101 (2001).

[63] L. Berthier and J. Kurchan, "Non-equilibrium glass transitions in driven and active matter," Nat. Phys. **9**, 310 (2013).

[64] J. Palacci, C. Cottin-Bizonne, C. Ybert, and L. Bocquet, "Sedimentation and effective temperature of active colloidal suspensions," Phys. Rev. Lett. **105**, 088304 (2010).

[65] P. Chvykov, T. A. Berrueta, A. Vardhan, W. Savoie, A. Samland, T. D. Murphey, K. Wiesenfeld, D. I. Goldman, and J. L. England, "Low rattling: A predictive principle for self-organization in active collectives," Science **371**, 90–95 (2021).

[66] D. A. Egolf, "Equilibrium regained: From nonequilibrium chaos to statistical mechanics," Science **287**, 101–104 (2000).

[67] J. S. Dahler and L. E. Scriven, "Angular momentum of continua," Nature **192**, 36–37 (1961).

[68] R. F. Snider and K. S. Lewchuk, "Irreversible thermodynamics of a fluid system with spin," J. Chem. Phys. **46**, 3163–3172 (1967).

[69] D. J. Evans, "On the generalized hydrodynamics of polyatomic fluids," Mol. Phys. **32**, 1171–1176 (1976).

[70] P. Schofield and J. R. Henderson, "Statistical mechanics of inhomogeneous fluids," Proc. R. Soc. A **379**, 231–246 (1982).

[71] I. Goldhirsch, "Stress, stress asymmetry and couple stress: from discrete particles to continuous fields," Granul. Matter **12**, 239–252 (2010).

[72] T. Harada and S.-i. Sasa, "Equality connecting energy dissipation with a violation of the fluctuation-response relation," Phys. Rev. Lett. **95**, 130602 (2005).

[73] É. Fodor, C. Nardini, M. E. Cates, J. Tailleur, P. Visco, and F. van Wijland, "How far from equilibrium is active matter?" Phys. Rev. Lett. **117**, 038103 (2016).

[74] J. Prost, J.-F. Joanny, and J. Parrondo, "Generalized fluctuation-dissipation theorem for steady-state systems," Phys. Rev. Lett. **103**, 090601 (2009).

[75] J. R. Gomez-Solano, A. Petrosyan, S. Ciliberto, R. Chetrite, and K. Gawędzki, "Experimental verification of a modified fluctuation-dissipation relation for a micron-sized particle in a nonequilibrium steady state," Phys. Rev. Lett. **103**, 040601 (2009).

[76] U. Seifert and T. Speck, "Fluctuation-dissipation theorem in nonequilibrium steady states," Europhys. Lett. **89**, 10007 (2010).

[77] S. D. Cengio, D. Levis, and I. Pagonabarraga, "Linear response theory and Green-Kubo relations for active matter," (2019), arXiv:1907.02560.

[78] A. Sarracino and A. Vulpiani, "On the fluctuation-dissipation relation in non-equilibrium and non-hamiltonian systems," Chaos **29**, 083132 (2019).

[79] S. Shankar and M. C. Marchetti, "Hidden entropy production and work fluctuations in an ideal active gas," Phys. Rev. E **98**, 020604 (2018).

[80] A. Puglisi, A. Baldassarri, and A. Vulpiani, "Violation of the einstein relation in granular fluids: the role of correlations," J. Stat. Mech.: Theory Exp. **2007**, P08016–P08016 (2007).

[81] P. Visco, "Work fluctuations for a brownian particle between two thermostats," J. Stat. Mech.: Theory Exp. **2006**, P06006–P06006 (2006).

[82] J. M. Horowitz and T. R. Gingrich, "Thermodynamic uncertainty relations constrain non-equilibrium fluctuations," Nat. Phys. **16**, 15–20 (2019).

[83] S. Sternberg, *Group Theory and Physics* (Cambridge University Press, 1995).

[84] H. Mori, "Transport, collective motion, and brownian motion," Prog. Theor. Exp. Phys. **33**, 423–455 (1965).

[85] S. Nakajima, "On quantum theory of transport phenomena," Prog. Theor. Exp. Phys. **20**, 948–959 (1958).

[86] R. Zwanzig, "Ensemble method in the theory of irreversibility," J. Chem. Phys. **33**, 1338–1341 (1960).

[87] T. Ihle and D. M. Kroll, "Stochastic rotation dynamics. i. formalism, galilean invariance, and green-kubo relations," Phys. Rev. E **67**, 066705 (2003).

[88] J. A. Krommes, "Projection-operator methods for classical transport in magnetized plasmas. part 1. linear response, the braginskii equations and fluctuating hydrodynamics," J. Plasma Phys. **84**, 925840401 (2018).

[89] Y. Feng, J. Goree, B. Liu, and E. G. D. Cohen, "Green-kubo relation for viscosity tested using experimental data for a two-dimensional dusty plasma," Phys. Rev. E **84**, 046412 (2011).

[90] Z. Haralson and J. Goree, "Overestimation of viscosity by the green-kubo method in a dusty plasma experiment," Phys. Rev. Lett. **118**, 195001 (2017).

[91] D. Banerjee, A. Souslov, and V. Vitelli, "Hydrodynamic correlation functions of chiral active fluids," (2020), arXiv:2005.00621.